Electronic properties and reactivity of Pt-doped carbon nanotubes†

Wei Quan Tian,‡ Lei Vincent Liu and Yan Alexander Wang*

Received 17th March 2006, Accepted 24th April 2006
First published as an Advance Article on the web 19th May 2006
DOI: 10.1039/b604032m

The structures of the (5,5) single-walled carbon nanotube (SWCNT) segments with hemispheric carbon cages capped at the ends (SWCNT rod) and the Pt-doped SWCNT rods have been studied within density functional theory. Our theoretical studies find that the hemispheric cages introduce localized states on the caps. The cap-Pt-doped SWCNT rods can be utilized as sensors because of the sensitivity of the doped Pt atom. The Pt-doped SWCNT rods can also be used as catalysts, where the doped Pt atom serves as the enhanced and localized active center on the SWCNT. The adsorptions of C_2H_4 and H_2 on the Pt atom in the Pt-doped SWCNT rods reveal different adsorption characteristics. The adsorption of C_2H_4 on the Pt atom in all of the three Pt-doped SWCNT rods studied (cap-end-doped, cap-doped, and wall-doped) is physisorption with the strongest interaction occurring in the middle of the sidewall of the SWCNT. On the other hand, the adsorption of H_2 on the Pt atom at the sidewall of the SWCNT is chemisorption resulting in the decomposition of H_2, and the adsorption of H_2 at the hemispheric caps is physisorption.

I. Introduction

Since the discovery of the single-walled carbon nanotube (SWCNT),[1] experimental and theoretical investigations on the chemical[2,3] and physical[4,5] properties of the SWCNT have been growing rapidly due to its potential applications[6] in molecular electronics,[7] chemical sensor,[8] vacuum electronic devices,[9] field emission flat panel display,[10] catalysis,[11] and optics.[12]

The SWCNT can be visualized as a roll of the graphite sheet and can be classified as metallic, narrow-gap and moderate-gap semiconducting nanotubes according to the wrapping vectors (m,n).[13] As shown in Scheme 1, nanotubes are characterized with a chiral vector ($\boldsymbol{AB} = ma + nb$) in which nanotubes are wrapped and a translation vector in which nanotubes elongate. If $n - m = 3q$ (with integral m, n, and q), the nanotube is metallic. Otherwise, it is semiconducting with a band gap.[13b] There are further detailed classifications of nanotubes with respect to the conductance according to the "$n - m$ rules".[13]

As one-dimensional (1-D) rolled graphite sheets, nanotubes display different electronic properties from those of planar graphite sheets and fullerenes: the electronic properties of nanotubes can be controlled by their diameters with different hybridization effects.[5a] For example, the pyramidization of nanotubes is different from fullerenes and there exists π-orbital misalignment between adjacent pairs of conjugated carbon atoms,[2a] which renders different reactivity of nanotubes from fullerenes and among nanotubes of various diameters.[2a,5e,14] Chemical reactions can take place on the sidewall of the nanotubes[15] or at the ends of the nanotubes.[15j,15k,16] In spite of numerous studies, the reactivity of the SWCNT is still not clear and deserves further investigation.[17]

Partial changes in the nanotube structure through vacancy,[18] doping with other elements (replacement of the carbon atoms on the SWCNT to produce the hetero SWCNT),[19] and distortion[20] can modify the electronics and reactivity of the nanotubes to some degree.[18g,19c] It has been found that substituting a carbon atom by a metal atom in fullerenes[21] renders the metal atom as an active center in chemical reactions.[21e,22] As a pseudo 1-D system with tube structure, the SWCNT with defects and doping can serve as a catalyst for gas-phase and liquid-phase reactions: the reactants enter from one end of an open SWCNT, the reaction is catalyzed at the defect or doping sites of the SWCNT, and the products exit from the other end of the open SWCNT. A good understanding of the electronic structure of the perfect, defected, and doped SWCNTs helps to comprehend the reactivity of such SWCNTs and to utilize such SWCNTs in chemical reactions.

In this work, we will study the structures and reactivity of the hetero SWCNTs (HSWCNTs) to shed some light on the reactivity of such HSWCNTs and their possible applications. Unlike most main group element doped HSWCNTs,[19] the HSWCNTs we study here are the transition-metal doped (more specifically, precious-metal Pt doped) HSWCNTs.

II. Models and computational details

The model for the SWCNT is chosen to be the (5,5) armchair metallic SWCNT with two hemispheric caps, which are the

Department of Chemistry, University of British Columbia, Vancouver, BC V6T 1Z1, Canada. E-mail: yawang@chem.ubc.ca
† The HTML version of this article has been enhanced with colour images.
‡ Permanent address: State Key Laboratory of Theoretical and Computational Chemistry, Institute of Theoretical Chemistry, Jilin University, Changchun, Jilin 130023, China.

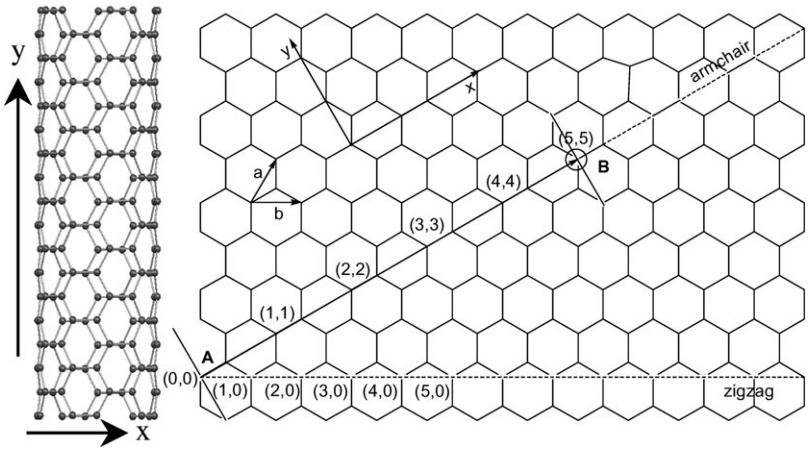

Scheme 1 Illustration of possible wrappings of the graphite sheet to the SWCNTs. Structure of the (5,5) SWCNT is shown on the left. The *x*-axis is the wrapping direction and the *y*-axis is the elongation direction. ***AB*** is the chiral vector.

half spheres of the fullerene. The open ends of the SWCNT were found to be active centers in many reactions, *e.g.* oxidation of the SWCNT,[16b] and the structure of the open ends goes through bond–distance reconstruction.[3i] No end-localized state has been found at energies near the Fermi surface for the open-end SWCNT.[3i] On the contrary, the caps in the capped nanorod were predicted to be important for the electronic properties of the nanorod[3d] and there exist electronic states localized on the caps[4a,23] because of the less stable pentagons,[24] despite that there is no significant contributions to the highest occupied molecular orbital (HOMO) and the lowest unoccupied molecular orbital (LUMO) of the nanorod from the caps.[3c] However, the differences in curvature and π bonding distinguish the chemical properties of fullerenes and the SWCNTs[2a] and thus divide the nanorod into at least two regions: the caps and the sidewall.

The structures of the (5,5) SWCNT rod and the Pt-doped (5,5) SWCNT rod with substitutions at the middle of the sidewall and at one of the end caps are studied with density functional theory (DFT).[25] Becke's exchange functional (B)[26] and Perdew's correlation functional (PW91)[27] based on the generalized gradient approximations are employed in structure optimization and property prediction. Pople's 6-31G[28] Gaussian basis set is used for carbon atoms and the relativistic 18-electron Los Alamos National Laboratory (LANL2DZ) effective core pseudopotential[29] with the basis set (3s3p2d) is used for the Pt atom. Because of its better predictive ability of relative energies,[30] the hybrid DFT method B3LYP[31] with the smaller LANL2MB[29] basis set is used for the geometry optimizations of the adsorptions of C_2H_4 and H_2 on the Pt-doped SWCNTs and the absorption energies are further refined by single-point energy calculations with the bigger LANL2DZ basis set. Partial charge analysis is performed with the natural bond orbitals (NBOs).[32] The geometries of all the Pt-doped nanorods are reoptimized with B3LYP/LNL2MB. The Gaussian 03[33] quantum chemical package is employed for all calculations in the present work.

III. Results and discussions

1. Perfect SWCNT rods

Fig. 1 and 2 display the geometries of the two (5,5) SWCNT rods, C_{170} and C_{180}, with D_{5h} and D_{5d} symmetries, and their density of states (DOS) and local density of states (LDOS), respectively. The DOS displays the overall electronic structure of a system, while the LDOS shows the electronic structure of a particular region and indicates the contribution of the atoms in that particular region to the overall DOS. The plots of the DOS and the LDOS above zero are for the discussion of the chemistry of the systems hereafter.

The similarity of the DOS and the LDOS of these two SWCNT rods is expected, since only one additional circular *cis*-polyene chain does not significantly change the electronic structure from C_{170} to C_{180}. Previous studies also found similarity in the HOMO–LUMO gaps of the (5,5) SWCNT rods, C_{170} and C_{180}.[3d] Fig. 1 and 2 also exhibit the LDOS of the *cis*-polyene chains in C_{170} and C_{180} along the SWCNT axis and the LDOS of the cap (a hemisphere of C_{60}). The shapes of the LDOS of different layers are similar at the frontier molecular orbital (MO) region, which indicates delocalization of the frontier MOs of the SWCNT rods. The contributions to the HOMO, the LUMO, and other occupied frontier MOs from the caps are not significant; the contributions to the HOMO and the LUMO of C_{170} and C_{180} are mainly from the sidewalls of the SWCNTs. The conspicuous contributions to the DOS from the LDOS of the cap lie about 1.0 eV below the HOMO and 0.5 eV above the LUMO, as indicated in Fig. 1 and 2.

The MOs give detailed information about the contributions of the LDOS from each layer to the DOS of the SWCNT rod. The occupied and unoccupied frontier MOs for the SWCNT rods C_{170} and C_{180} are plotted in Fig. 3 and 4, respectively. The highest four occupied MOs of C_{170} and C_{180} are π orbitals with contributions from the sidewalls of the SWCNT rods and are delocalized on the sidewalls. The occupied MOs with major contribution from the caps lie about 1 eV below the HOMO, similar to the picture manifested by the LDOS of the cap in

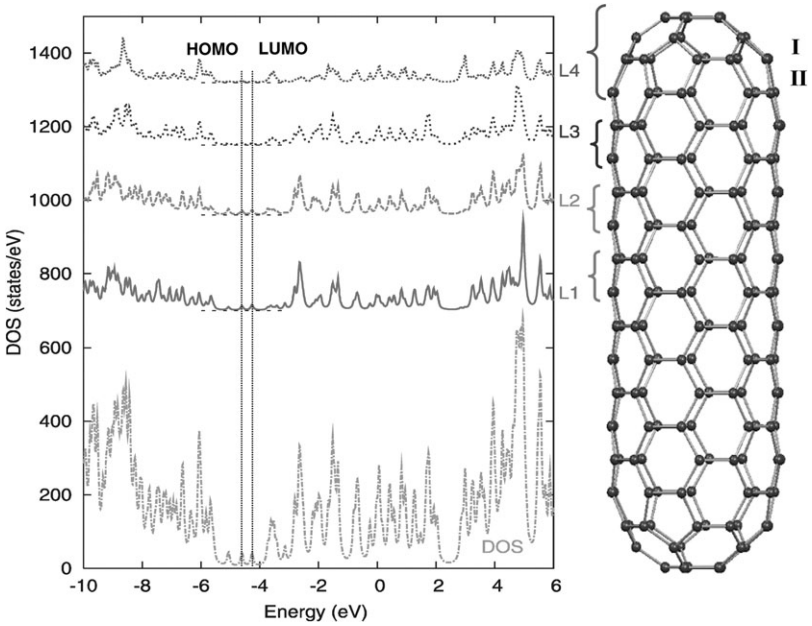

Fig. 1 Density of states and local density of states for nanorod C_{170} with the D_{5h} symmetry. HOMO is the highest occupied molecular orbital with orbital energy −4.61 eV, and LUMO is the lowest unoccupied molecular orbital with orbital energy −4.26 eV. L1, L2, L3, and L4 are the local densities of states for each specified layer of atoms of C_{170} as marked on the structure.

Fig. 1 and 2. The HOMO and the LUMO have sole contributions from the sidewall of the SWCNT. The lowest two unoccupied MOs of C_{170} and C_{180} are delocalized π orbitals of the sidewalls of the SWCNTs and are followed by four (two two-fold degenerate) localized MOs on the caps. The patterns of the HOMO and the LUMO in C_{170} are different from their counterparts in C_{180}. Such a pattern change was observed for shorter SWCNT rods before.[3c]

From the MOs, one can infer that, when reacting with strong electron acceptors, the SWCNT rods C_{170} and C_{180} will donate electrons from the sidewalls of the SWCNTs to the electron acceptors. When C_{170} and C_{180} accept electrons, the first four electrons will go to the middle of the sidewalls of the SWCNTs, and any extra (up to eight) electrons will go to the caps. From the frontier occupied MOs of C_{170} and C_{180}, one cannot see clearly the separation of the electronic structure of

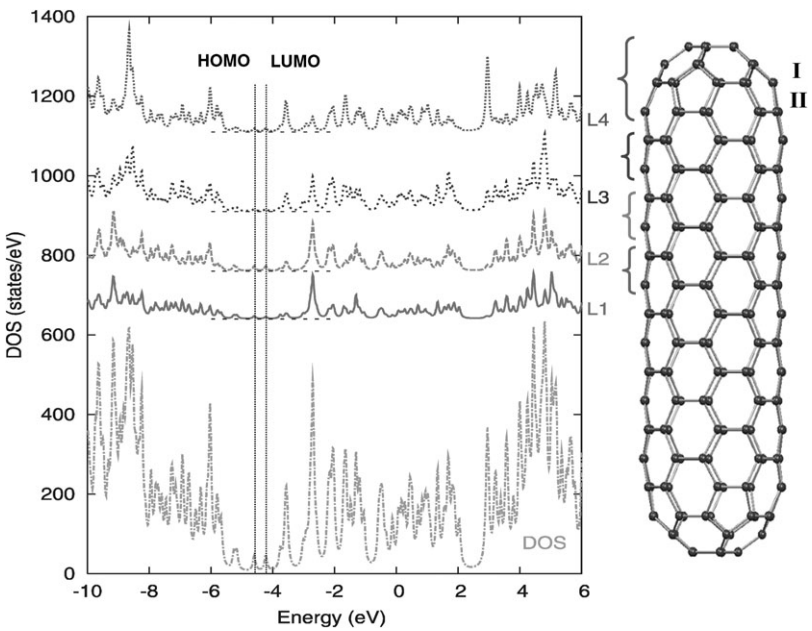

Fig. 2 Density of states and local density of states for nanorod C_{180} with the D_{5d} symmetry. HOMO is the highest occupied molecular orbital with orbital energy −4.60 eV, and LUMO is the lowest unoccupied molecular orbital with orbital energy −4.23 eV. L1, L2, L3, and L4 are the local densities of states for each specified layer of atoms of C_{180} as marked on the structure.

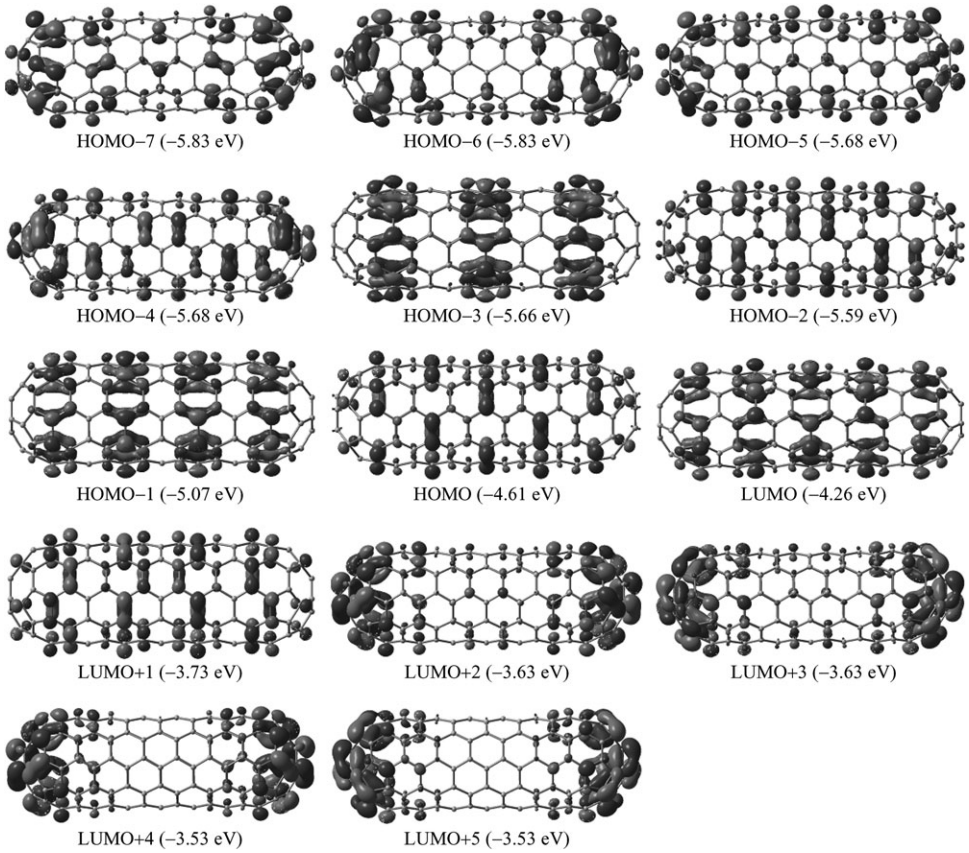

Fig. 3 Frontier orbitals of nanorod C_{170} with the D_{5h} symmetry. HOMO–n (p eV) is the nth orbital below the HOMO with orbital energy p eV. LUMO+m (q eV) is the mth orbital above the LUMO with orbital energy q eV.

the caps from the sidewall of the SWCNT, though there exists some gradual geometric change from the caps to the sidewall.[34] The delocalized MOs on the sidewall of the SWCNT rods extend to the ridge of the pentagons of the caps. The pentagon regions have 6–6 (between two hexagons) and 6–5 (between a hexagon and a pentagon) CC bond alternation, similar to that in C_{60}. From the MOs of C_{170} and C_{180}, one can infer that the electronic structure on the caps is localized and the geometric (topological) role of the caps can be the dominant factor for determining the electronic properties of the SWCNT rods.[34]

The atoms on the last layer of L4 (II in Fig. 1 and 2) have the largest negative charge in C_{180} and a large negative charge in C_{170}. In chemical reactions, this layer is reactive toward electron acceptors and can be treated as a bridge between the sidewall and the cap of a SWCNT rod. The middle layers of the sidewall of the SWCNT rod have a positive charge.

For C_{170}, the vertical ionization potential (IP) and electron affinity (EA) are 5.86 and 2.89 eV, respectively.

Due to the similarity of the electronic and geometric structures of C_{170} and C_{180}, we will focus on C_{170} and its doping derivatives for the rest of the investigation.

2. Pt-doped SWCNT rods

For C_{170}, NBO partial charge analysis indicates that the five atoms connecting to the top pentagon of the cap have the largest negative charges and the atoms of the next layer (I in Fig. 1) have the largest positive charge. Thus, the caps can be chemical reaction centers. Substitution of the carbon atoms in the cap by other elements will change the chemical selectivity and sensitivity of the SWCNT rod in catalytic reactions. Replacing one carbon atom with a Pt atom in the end pentagon, in the next layer, or on the sidewall of C_{170} results in three Pt-doped SWCNT rods: the cap-end-doped $C_{169}Pt(ce)$, the cap-doped $C_{169}Pt(c)$, and the wall-doped $C_{169}Pt(w)$, as shown in Fig. 5, 6, and 7. Single-point calculations at the BPW91/6-31G level of theory predict that $C_{169}Pt(ce)$ is the most stable nanorod: the total energies of $C_{169}Pt(c)$ and $C_{169}Pt(w)$ are 0.8 and 17.9 kcal mol^{-1} higher, respectively. Evidently, the cap-doped SWCNTs are more stable than the wall-doped SWCNT, because of the relaxation of the constraint on the cap through doping. The total energy of the triplet electronic state of the Pt-doped nanorod is found to be higher than that of the singlet, *i.e.* the ground state of the Pt-doped nanorod is singlet.

2.A. Cap-end-doped $C_{169}Pt(ce)$. Fig. 5 and 8 display the structure, the DOS, the LDOS, and the frontier MOs of $C_{169}Pt(ce)$. The Pt–C bond distances at the cap end are 2.01 Å and the other Pt–C bond distances are 1.96 Å. Clearly, the Pt atom points outwards along the translation direction of the SWCNT. The distortion of the SWCNT rod due to the Pt-doping is localized on the pentagons and hexagons around Pt.

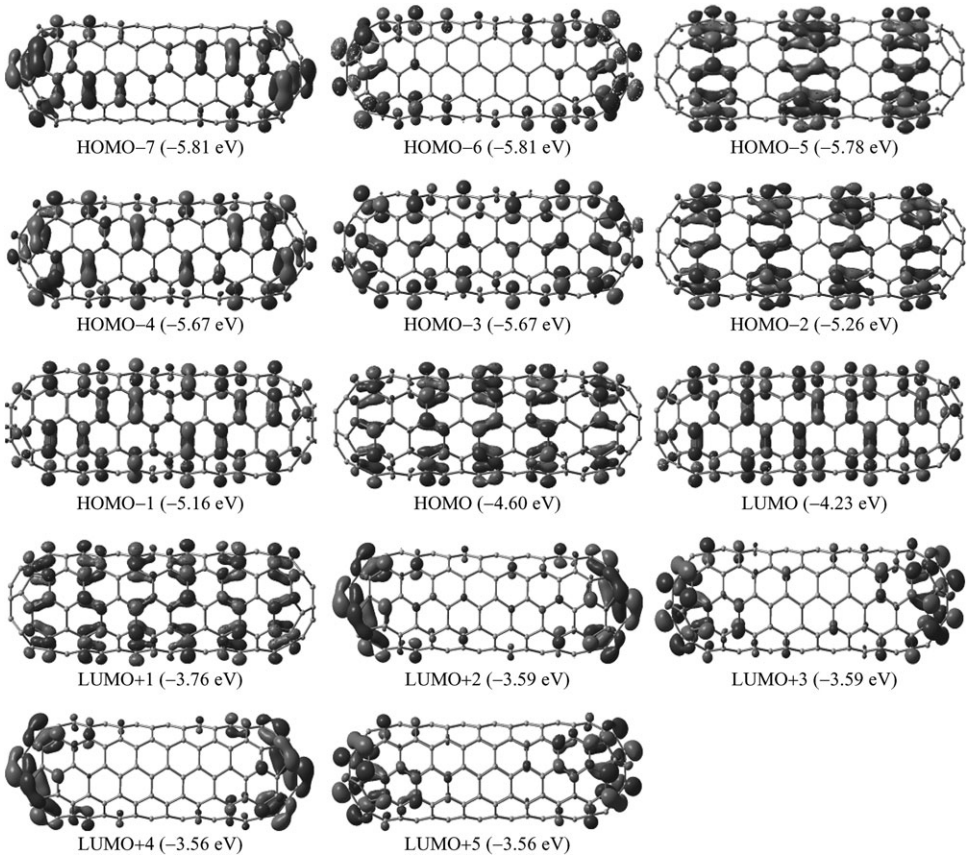

Fig. 4 Frontier orbitals of nanorod C_{180} with the D_{5d} symmetry. HOMO–n (p eV) is the nth orbital below the HOMO with orbital energy p eV. LUMO+m (q eV) is the mth orbital above the LUMO with orbital energy q eV.

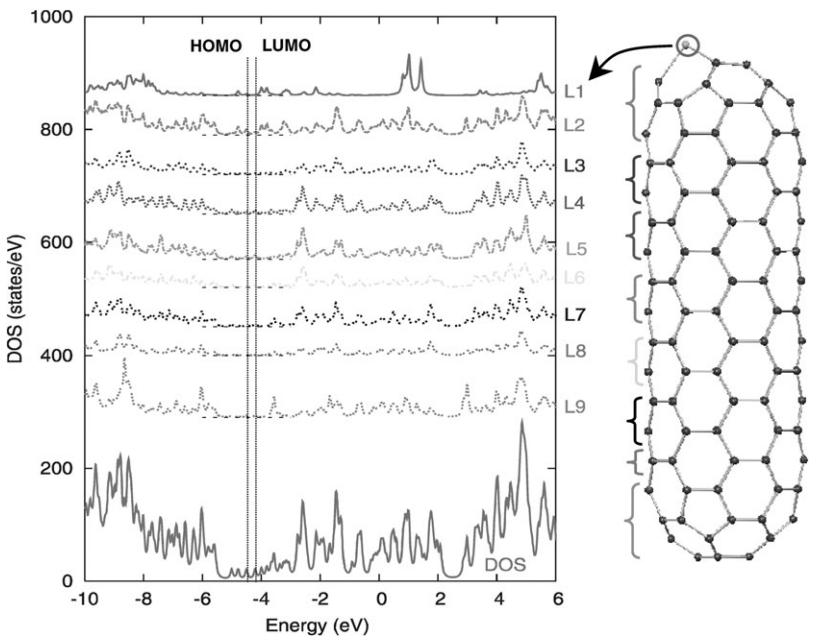

Fig. 5 Density of states and local density of states for the Pt cap-end-doped nanorod $C_{169}Pt(ce)$ with the C_s symmetry. HOMO is the highest occupied molecular orbital with orbital energy −4.51 eV, and LUMO is the lowest unoccupied molecular orbital with orbital energy −4.21 eV. L1, L2, L3, L4, L5, L6, L7, L8, and L9 are the local density of states for each specified layer of atoms of $C_{169}Pt(ce)$ as marked on the structure.

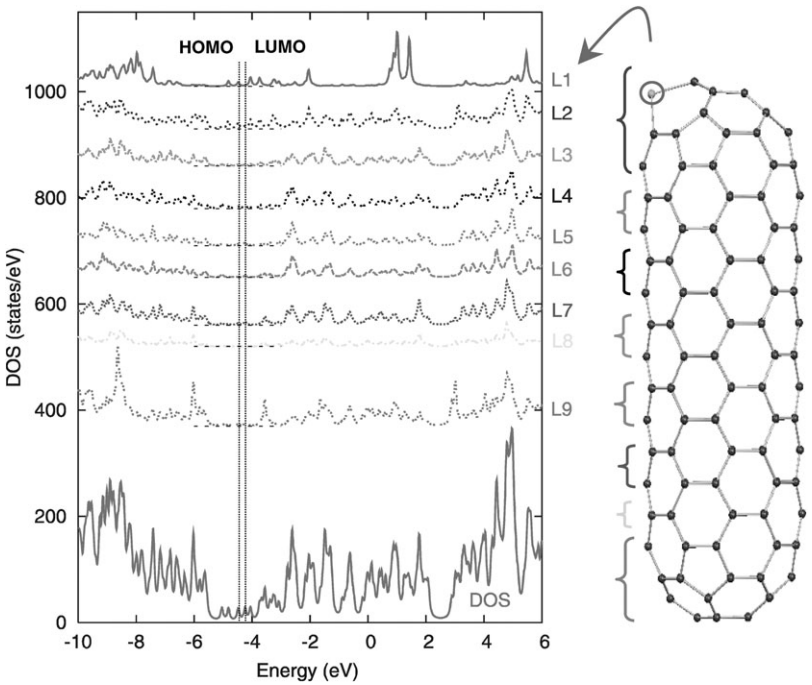

Fig. 6 Density of states and local density of states for the Pt cap-doped nanorod $C_{169}Pt(c)$ with the C_s symmetry. HOMO is the highest occupied molecular orbital with orbital energy −4.48 eV, and LUMO is the lowest unoccupied molecular orbital with orbital energy −4.25 eV. L1, L2, L3, L4, L5, L6, L7, L8, and L9 are the local density of states for each specified layer of atoms of $C_{169}Pt(c)$ as marked on the structure.

The overall DOS of $C_{169}Pt(ce)$ is similar to that of C_{170} with the D_{5h} symmetry. The doping of Pt produces more peaks in the DOS in the frontier MO region due to the introduction of the Pt 5d orbitals and the induced electronic structure change in the doped cap. The LDOS of L1 and L2 in Fig. 5 clearly indicates such changes. L1 (the LDOS of Pt) in Fig. 5 manifests the contribution of Pt to the DOS of $C_{169}Pt(ce)$. The LDOS of the remaining layers in Fig. 5 are similar to one another.

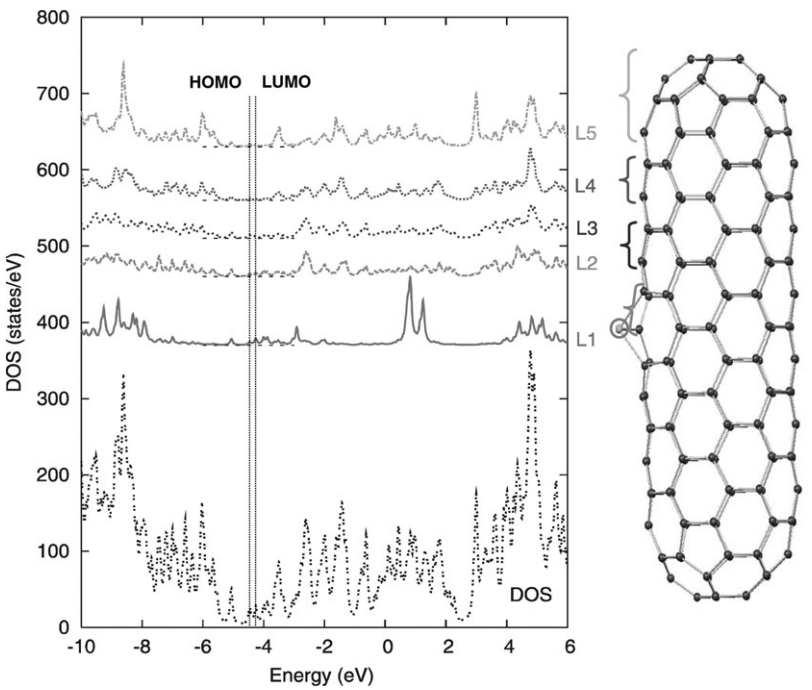

Fig. 7 Density of states and local density of states for the Pt wall-doped nanorod $C_{169}Pt(w)$ with the C_s symmetry. HOMO is the highest occupied molecular orbital with orbital energy −4.46 eV, and LUMO is the lowest unoccupied molecular orbital with orbital energy −4.26 eV. L1, L2, L3, L4, and L5 are the local densities of states for each specified layer of atoms of $C_{169}Pt(w)$ as marked on the structure.

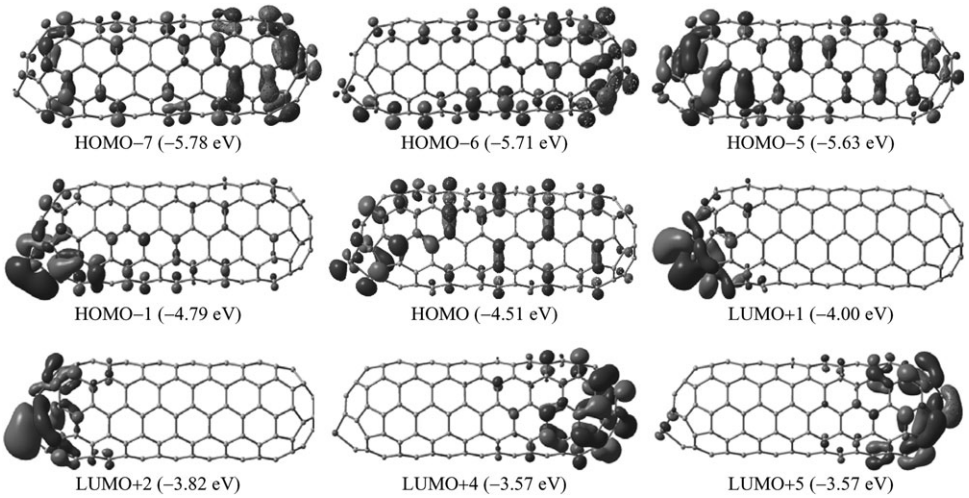

Fig. 8 Relevant frontier orbitals of the Pt cap-end-doped nanorod $C_{169}Pt$(ce) with the C_s symmetry. HOMO−n (p eV) is the nth orbital below the HOMO with orbital energy p eV. LUMO+m (q eV) is the mth orbital above the LUMO with orbital energy q eV.

The frontier MOs in Fig. 8 reveal details of the electronic structure of $C_{169}Pt$(ce). The HOMO of $C_{169}Pt$(ce) is similar to that of C_{170}, except for the significant contributions from Pt and its neighboring carbon atoms in $C_{169}Pt$(ce). The effect of Pt on the electronic structure of $C_{169}Pt$(ce) is also reflected in several other occupied MOs: the HOMO−1, the HOMO−5, the HOMO−6, and the HOMO−7. The HOMO−1 has some major contributions from the Pt 5d orbitals, which form d-p π bonds with the carbon atoms in the next layer. The geometric distortion in $C_{169}Pt$(ce) induces single and double CC bond alteration around Pt, which is reflected in the strong π bonding around the doped cap in the HOMO−5. The symmetry of the π bonds in the HOMO−7, the HOMO−6, and the HOMO−5 (corresponding to the HOMO−7, the HOMO−6, and the HOMO−5 in C_{170}) is destroyed in $C_{169}Pt$(ce), resulting in concentrated π bonding on one end cap, as clearly shown in Fig. 8. The LUMO of $C_{169}Pt$(ce) is very similar to that of C_{170}. The next two unoccupied MOs, the LUMO+1 and the LUMO+2, of $C_{169}Pt$(ce) are mainly from the 5d orbitals of Pt, and the contribution to these two unoccupied MOs from the undoped cap diminishes. According to the MOs of $C_{169}Pt$(ce), it is quite clear that the reactive center in $C_{169}Pt$(ce) is around the location of Pt.

The Pt atom can donate electrons to electron acceptors and its empty 5d orbitals can accept electrons from electron donors, *e.g.* in reaction with gases like H_2, C_2H_4, CO, NH_3, NO, *etc.* NBO partial charge analysis indicates that Pt transfers about 0.80 electrons (0.40 electrons from 6s and 0.40 electrons from 5d) to nearby carbons: the electronic configuration of the Pt atom is essentially [core]$5d^{8.60}6s^{0.60}$. The carbon atom connecting to Pt in the second layer from the doped cap end has the largest negative charge, −0.22.

The vertical IP and EA of $C_{169}Pt$(ce) are 5.45 and 3.40 eV, respectively.

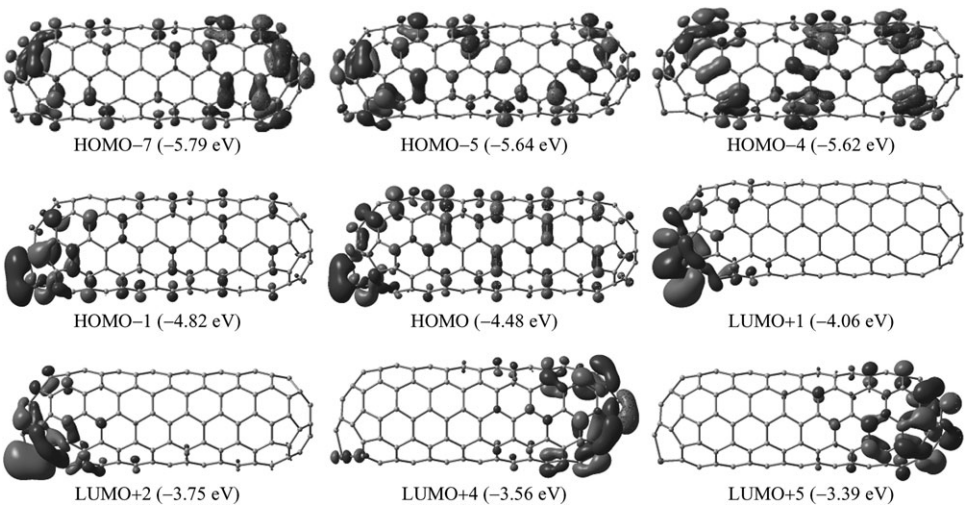

Fig. 9 Frontier orbitals of the Pt cap-doped nanorod $C_{169}Pt$(c) with the C_s symmetry. HOMO−n (p eV) is the nth orbital below the HOMO with orbital energy p eV. LUMO+m (q eV) is the mth orbital above the LUMO with orbital energy q eV.

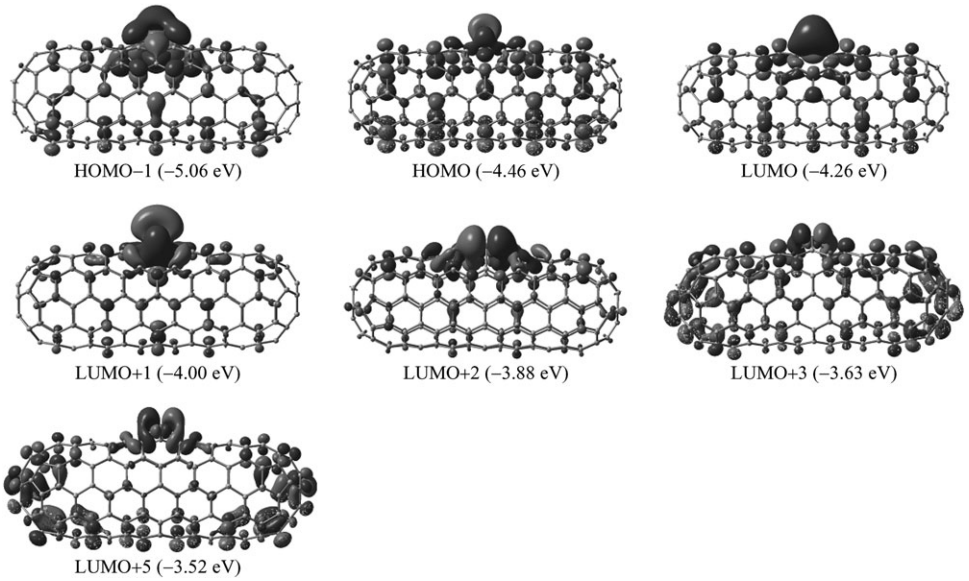

Fig. 10 Relevant frontier orbitals of the Pt wall-doped nanorod $C_{169}Pt(w)$ with the C_s symmetry. HOMO−n (p eV) is the nth orbital below the HOMO with orbital energy p eV. LUMO+m (q eV) is the mth orbital above the LUMO with orbital energy q eV.

2.B. Cap-doped $C_{169}Pt(c)$. Fig. 6 shows that the DOS and the LDOS of each layer of atoms of $C_{169}Pt(c)$ are very similar to those of $C_{169}Pt(ce)$. The structure of $C_{169}Pt(c)$ is also similar to that of $C_{169}Pt(ce)$, except for the region around Pt. The Pt−C bond distance between Pt and the carbon atom in the top pentagon is 1.97 Å; the other two equivalent Pt–C bond distances are 2.00 Å. The long Pt−C bonds make the carbon atom of the top pentagon connected to Pt slightly point out of the pentagon, as shown in Fig. 6. The frontier MOs of $C_{169}Pt(c)$, as shown in Fig. 9, are very similar to those of $C_{169}Pt(ce)$ in Fig. 8. The noticeable difference is that Pt contributes to the HOMO of $C_{169}Pt(c)$ more than it does in $C_{169}Pt(ce)$, which will enhance the reactivity of Pt in $C_{169}Pt(c)$. The electronic configuration of the Pt atom is essentially $[core]5d^{8.63}6s^{0.60}$. The partial charge of Pt is 0.77 and the carbon atom connecting to Pt in the top pentagon has the largest negative partial charge, −0.25. The vertical IP and EA of $C_{169}Pt(c)$ are 5.49 and 3.21 eV, respectively.

2.C. Wall-doped $C_{169}Pt(w)$. Fig. 7 and 10 display the DOS, the LDOS of each layer, and the frontier MOs of $C_{169}Pt(w)$. The DOS of $C_{169}Pt(w)$ around the frontier MO region is different from those of $C_{169}Pt(ce)$ and $C_{169}Pt(c)$: the contribution to the DOS at the frontier MO region from Pt has noticeably increased in $C_{169}Pt(w)$. The LDOS of Pt indicates that Pt contributes significantly to the DOS at the frontier MO

Table 1 The relative stabilities of the Pt-doped nanorods and the adsorption energies of C_2H_4 and H_2 on the Pt-doped nanorods. The minus sign indicates the release of the heat of formation upon the adsorption. All energies are in kcal mol^{-1}

Adsorbate	Level of theory	$C_{169}Pt(ce)$	$C_{169}Pt(c)$	$C_{169}Pt(w)$
None	BPW/6-31G	0.0	0.8	17.9
	B3LYP/Lanl2mb	0.0	2.4	28.6
	B3LYP/Lanl2dz	0.0	3.3	26.3
C_2H_4	B3LYP/Lanl2mb	−22.4	−23.5	−19.2
	B3LYP/Lanl2dz	−20.6	−22.2	−14.7
H_2	B3LYP/Lanl2mb	−2.1	−2.3	−10.7
	B3LYP/Lanl2dz	−2.8	−3.0	−10.9

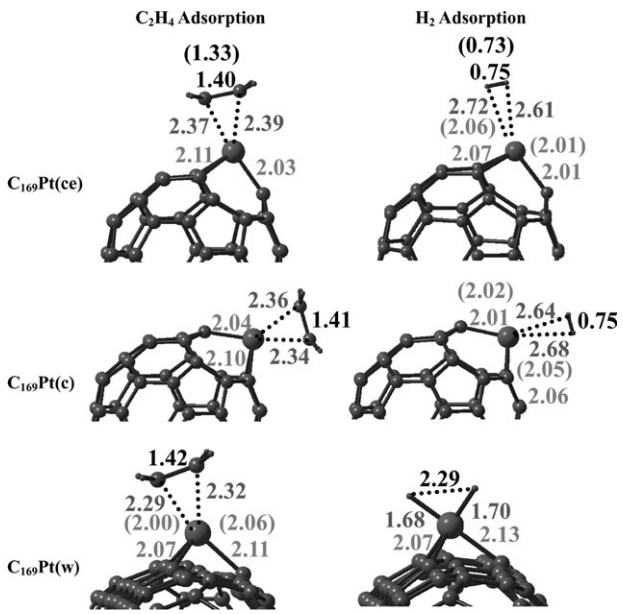

Fig. 11 The relevant bond distances (in Å) of the adsorptions of C_2H_4 and H_2 on the Pt atom in the Pt-doped nanorods ($C_{169}Pt$). The Pt atom is the big ball. The C═C bond distances in the C_2H_4 adsorption are about 1.4 Å. The H–H bond distances in the H_2 adsorptions on $C_{169}Pt(ce)$ and $C_{169}Pt(c)$ and on $C_{169}Pt(w)$ are 0.75 and 2.29 Å, respectively. The PtC bond distances between Pt and the carbon atoms of C_2H_4 in the C_2H_4 adsorption are about 2.3 Å. The PtH bond distances in the H_2 adsorptions on $C_{169}Pt(ce)$ and $C_{169}Pt(c)$ and on $C_{169}Pt(w)$ are about 2.7 and 1.7 Å, respectively. The PtC bond distances between Pt and its nearest carbon atoms of the SWCNT are about 2.0 Å. The numbers in parentheses are the PtC bond distances of the isolated $C_{169}Pt$ without adsorption, the C═C bond distance in the isolated free C_2H_4, and the H–H bond distance of the isolated free H_2.

region in $C_{169}Pt(w)$. The introduction of Pt on the sidewall of the SWCNT also drastically changes the LDOS of its neighboring carbon layers, which can be vividly demonstrated by the comparison of the LDOS of L2 and L3 in Fig. 7 with L1 and L2 of C_{170} in Fig. 1. The LDOS contribution from each layer is also depicted by the frontier MOs, as shown in Fig. 10. From the HOMO−1 to the LUMO+3, Pt has significant contributions to each MO. The HOMO–LUMO gap (0.20 eV) of $C_{169}Pt(w)$ is smaller than those of C_{170} (0.35 eV), $C_{169}Pt(ce)$ (0.30 eV), and $C_{169}Pt(c)$ (0.23 eV). In chemical reactions, Pt will serve as various catalytic centers with flexible oxidation states capable of accepting and donating electrons. The electronic configuration of Pt is essentially $[core]5d^{8.63}6s^{0.54}$. The partial charge of Pt is 0.83. The partial charge of the carbon atom connecting to Pt in the symmetric plane is −0.18, where the Pt–C bond distance is 2.01 Å. The partial charges of the other two equivalent carbon atoms connecting to Pt are −0.10, and the two equivalent Pt–C bond distances are 1.95 Å. The vertical IP and EA of $C_{169}Pt(w)$ are 5.44 and 3.28 eV, respectively.

3. Adsorptions of C_2H_4 and H_2 on $C_{169}Pt$

From the EAs and IPs of C_{170} and the three Pt-doped nanorods, one can see that the doping of Pt enhances both the electron accepting and donating capacities of the doped nanorod. Thus, the doping of Pt certainly changes the chemical reactivity and regioselectivity of the SWCNT and broadens the field of application of the SWCNT rods in such areas as gas sensors.[35] Present studies have found that the change of structure and reactivity through the doping of Pt in the SWCNT is localized at the doping site.

To reveal the different reactivity of the Pt-doped SWCNTs, we are now studying adsorptions of C_2H_4 and H_2 on the Pt atom of the three Pt-doped SWCNTs. The relative stability of the Pt-doped SWCNTs and the adsorption energies of C_2H_4 and H_2 on the Pt-doped SWCNTs are collected in Table 1.

As can be seen from the bond distances at the adsorption site in Fig. 11, there is no significant structural change at the Pt-doped region for the adsorption of H_2 on the two

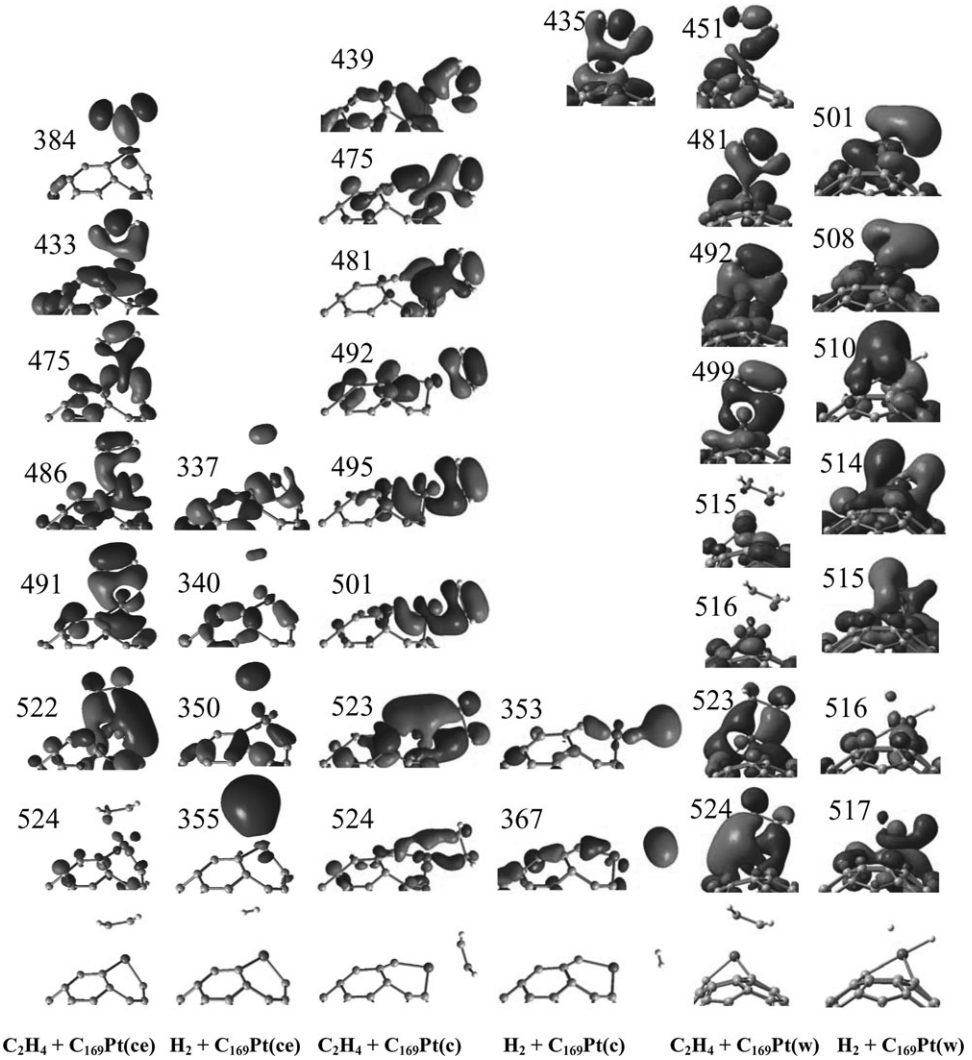

Fig. 12 Portions of the molecular orbitals relevant to the interaction of the adsorbates, C_2H_4 and H_2, with the three kinds of the Pt-doped nanorods, $C_{169}Pt(ce)$, $C_{169}Pt(c)$, and $C_{169}Pt(w)$. The numbers beside the molecular orbitals are the orbital indexes. The critical geometries of these structures are shown in Fig. 11.

cap-doped SWCNTs, as exemplified by the Pt–C bond distances. These two cases are physisorptions according to the H–H bond distance and the distances between H_2 and the SWCNT shown in Fig. 11 and the adsorption energies in Table 1. On the other hand, the adsorption of H_2 on the Pt atom in the middle of the nanorod $C_{169}Pt(w)$ is a chemical one. Obviously, the H–H bond is broken and the two hydrogen atoms form chemical bonds with Pt with bond lengths of *ca.* 1.70 Å. The distance between the two hydrogen atoms is 2.29 Å. This chemisorption releases about 10.0 kcal mol^{-1} energy, which is nearly five times the energy (about 2.0 $\sim$ 3.0 kcal mol^{-1}) released by the adsorption of H_2 on the Pt atom at the end cape of the SWCNT rods. The interaction between H_2 and Pt in the two physisorptions is mainly the electron transfer from the bonding orbital of H_2 to the empty 5d orbital of Pt, as indicated by the MOs in Fig. 12. Though the two hydrogen atoms in the adsorption on $C_{169}Pt(w)$ are separated, the interaction between these two hydrogen atoms remains strong, as revealed by the MO overlaps between them (Fig. 12).

The adsorption of C_2H_4 on the Pt atom in the three Pt-doped nanorods is physisorption with C–Pt distances *ca.* 2.30 Å. As the adsorption site changes from the end-caps of $C_{169}Pt(ce)$ and $C_{169}Pt(c)$ to the middle of the sidewall of $C_{169}Pt(w)$, the CC bond distance in C_2H_4 gets longer, and Pt–C bond distances between C_2H_4 and Pt get shorter, perhaps indicating the strength of the interaction between C_2H_4 and the Pt-doped SWCNTs in this ascending order: $C_{169}Pt(ce) < C_{169}Pt(c) < C_{169}Pt(w)$. However, this conclusion based on structure analysis alone does not agree with the data in Table 1: the adsorption energy of C_2H_4 is the smallest on $C_{169}Pt(w)$ and the largest on $C_{169}Pt(c)$. The trend of the adsorption strengths of C_2H_4 on the Pt-doped SWCNTs is the compromise of the weakening of the C=C double bond in C_2H_4, the electrostatic attraction between the two carbon atoms of C_2H_4 and Pt, and the repulsion between the C_2H_4 and the SWCNT. It is also interesting to note that the geometries of the adsorptions of C_2H_4 on the Pt atom at the end-cap of the Pt-doped SWCNTs are very similar to those on the Pt-doped fullerene, $C_{59}Pt$,[21e] which should possess similar adsorption strengths.

Overall, the adsorptions of H_2 and C_2H_4 get stronger as the adsorption site changes from the hemispheric cap to the sidewall of the SWCNT, as manifested by the relevant MOs in Fig. 12 and the adsorption energies in Table 1.

IV. Conclusions

Within DFT, the electronic structures and chemical reactivity of the SWCNT rods C_{170} and C_{180}, the Pt-doped SWCNT rods $C_{169}Pt(ce)$, $C_{169}Pt(c)$, and $C_{169}Pt(w)$ have been studied in detail. According to the analyses, we have reached the following conclusions:

1. There indeed exist localized electronic states on the caps of the SWCNT rods as confirmed by the DOS, the LDOS, and the frontier MOs. The circular *cis*-polyene chain between the cap and the sidewall of the SWCNT is chemically active.

2. The ground state of the Pt-doped SWCNT rod is a singlet.

3. The doping of Pt in the SWCNT rod results in localized electronic states at Pt, thus rendering Pt as the active center in chemical reactions, particularly for the wall-doped $C_{169}Pt(w)$. The Pt-doped SWCNT rod with Pt at the end of the cap, $C_{169}Pt(ce)$, can be used as a chemical sensor, since the doping of Pt enhances the sensitivity of the cap in interaction with the substrate due to the Pt 5d orbitals and the charge transfer from Pt to the carbon atoms. In Pt-doped SWCNT rods, Pt is essentially acting as Pt^+, because of the electron transfer of about one electron from Pt to the carbon atoms.

4. The doping of Pt in the middle of the sidewall of the nanorod has stronger interaction with the adsorbates (*e.g.*, H_2 and C_2H_4) than the nanorods with the doping of Pt at the hemispheric caps. This further suggests that the Pt-doped SWCNT has stronger adsorbing capacity than the Pt-doped fullerene. However, this phenomenon has to be investigated for systems involving other metals.

In summary, present DFT studies reveal that doping produces localized active centers, thus enhancing the chemical reactivity of the SWCNTs (with hemispherically capped ends). Our studies point to new directions for future applications of the SWCNTs in catalysis, chemic sensor, surface science, and nanotube chemistry.

Acknowledgements

The financial support from the Natural Sciences and Engineering Research Council (NSERC) of Canada is gratefully acknowledged. WestGrid and C-HORSE have provided the necessary computational resources. L.V.L. gratefully acknowledges the Gladys Estella Laird and the Charles A. McDowell fellowships from the Department of Chemistry at the University of British Columbia.

References

1 (*a*) S. Iijima and T. Ichihashi, *Nature*, 1993, **363**, 603; (*b*) D. S. Bethune, C.-H. Kiang, M. S. de Vries, G. Gorman, R. Savoy, J. Vazquez and R. Beyers, *Nature*, 1993, **363**, 605.

2 (*a*) S. Niyogi, M. A. Hamon, H. Hu, B. Zhao, P. Bhowmik, R. Sen, M. E. Itkis and R. C. Haddon, *Acc. Chem. Res.*, 2002, **35**, 1105; (*b*) T. Hermraj-Benny, S. Banerjee and S. S. Wong, *Chem. Mater.*, 2004, **16**, 1855; (*c*) J.-M. Nhut, P. Nguyen, C. Pham-Huu, N. Keller and M.-J. Ledoux, *Catal. Today*, 2004, **91**, 91; (*d*) J. Zhang, H. Zou, Q. Qing, Y. Yang, Q. Li, Z. Liu, X. Guo and Z. Du, *J. Phys. Chem. B*, 2003, **107**, 3712.

3 (*a*) T. Yamabe, M. Imade, M. Tanaka and T. Sato, *Synth. Met.*, 2001, **117**, 61; (*b*) X. Lu, F. Tian, Y. Feng, X. Xu, N. Wang and Q. Zhang, *Nano Lett.*, 2002, **2**, 1325; (*c*) J. Li, Y. Zhang and M. Zhang, *Chem. Phys. Lett.*, 2002, **364**, 328; (*d*) J. Cioslowski, N. Rao and D. Moncrieff, *J. Am. Chem. Soc.*, 2002, **124**, 8485; (*e*) T. Kar, B. Akdim, X. Duan and R. Pachter, *Chem. Phys. Lett.*, 2004, **392**, 176; (*f*) M. Zhao, Y. Xia, J. P. Lewis and L. Mei, *J. Phys. Chem. B*, 2004, **108**, 9599; (*g*) S. Gustavsson, A. Rosén, H. Grennberg and K. Bolton, *Chem.-Eur. J.*, 2004, **10**, 2223; (*h*) E. Joselevich, *ChemPhysChem*, 2004, **5**, 619; (*i*) Z. Zhou, M. Steigerwald, M. Hybertsen, L. Brus and R. Friesner, *J. Am. Chem. Soc.*, 2004, **126**, 3597; (*j*) T. Yumura, K. Hirahara, S. Bandow, K. Yoshizawa and S. Iijima, *Chem. Phys. Lett.*, 2004, **386**, 38.

4 (*a*) D. L. Carroll, P. Redlich, P. M. Ajayan, J. C. Charlier, X. Blase, A. De Vita and R. Car, *Phys. Rev. Lett.*, 1997, **78**, 2811; (*b*) Z. Klusek, P. Kowalczyk and P. Byszewski, *Vacuum*, 2001, **63**,

145; (*c*) M. Shiraishi and M. Ata, *Synth. Met*., 2002, **128**, 235; (*d*) K. A. Dean and B. R. Chalamala, *J. Vac. Sci. Technol., B*, 2003, **21**, 868; (*e*) H. Kim, J. Lee, S.-J. Kahng, Y.-W. Son, S. B. Lee, C.-K. Lee, J. Ihm and Y. Kuk, *Phys. Rev. Lett*., 2003, **90**, 216107.
5 (*a*) X. Blase, L. X. Bbenedict, E. L. Shirley and S. G. Louie, *Phys. Rev. Lett*., 1994, **72**, 1878; (*b*) Y. H. Lee, S. G. Kim and D. Tománek, *Phys. Rev. Lett*., 1997, **78**, 2393; (*c*) T. Yaguchi and T. Ando, *J. Phys. Soc. Jpn*., 2001, **70**, 1327; (*d*) T. Yaguchi and T. Ando, *J. Phys. Soc. Jpn*., 2002, **71**, 2224; (*e*) J. Jiang, J. Dong and D. Y. Xing, *Phys. Rev. B*, 2002, **65**, 245418; (*f*) S. Compernolle, L. Chibotaru and A. Ceulemans, *J. Chem. Phys*., 2003, **119**, 2854; (*g*) L. Chico and W. Jasklski, *Phys. Rev. B*, 2004, **69**, 085406; (*h*) G. Y. Guo, K. C. Chu, D.-S. Wang and C.-G. Duan, *Phys. Rev. B*, 2004, **69**, 205416.
6 P. M. Ajayan and O. Z. Zhou, in *Carbon Nanotubes Synthesis, Structure, Properties, and Applications*, ed. M. S. Dresselhaus, G. Dresselhaus and Ph. Avoutis, Springer, Berlin, 2001.
7 (*a*) P. Avouris, *Acc. Chem. Res*., 2002, **35**, 1026; (*b*) R. D. Antonov and A. T. Johnson, *Phys. Rev. Lett*., 1999, **83**, 3274; (*c*) M. S. Fuhrer, J. Nygård, L. Shih, M. Forero, Y.-G. Yoon, M. S. C. Mazzoni, H. J. Choi, J. Ihm, S. G. Louie, A. Zettl and P. L. McEuen, *Science*, 2000, **288**, 494.
8 (*a*) J. Kong, N. R. Franklin, C. Zhou, M. G. Chapline, S. Peng, K. Cho and H. Dai, *Science*, 2000, **287**, 622; (*b*) P. G. Collins, K. Bradley, M. Ishigami and A. Zettl, *Science*, 2000, **287**, 1801; (*c*) A. Goldoni, R. Larciprete, L. Petaccia and S. Lizzit, *J. Am. Chem. Soc*., 2003, **125**, 11329.
9 O. Zhou, H. Shimoda, B. Gao, S. Oh, L. Fleming and G. Yue, *Acc. Chem. Res*., 2002, **35**, 1045.
10 W. B. Choi, D. S. Chung, J. H. Kang, H. Y. Kim, Y. W. Jin, I. T. Han, Y. H. Lee, J. E. Jung, N. S. Lee, G. S. Park and J. M. Kim, *Appl. Phys. Lett*., 1999, **75**, 3129.
11 P. Serp, M. Corrias and P. Kalck, *Appl. Catal., A*, 2003, **253**, 337.
12 (*a*) S. Botti, R. Ciardi, L. De Dominicis, L. S. Asilyan, R. Fantoni and T. Marolo, *Chem. Phys. Lett*., 2003, **378**, 117; (*b*) S. Tatsuura, M. Furuki, Y. Sato, I. Iwasa, M. Tian and H. Mitsu, *Adv. Mater*., 2003, **15**, 534; (*c*) S. Y. Set, H. Yaguchi, Y. Tanaka and M. Jablonski, *J. Lightwave Technol*., 2004, **22**, 51; (*d*) A. G. Rozhin, Y. Sakakibara, M. Tokumoto, H. Kataura and Y. Achiba, *Thin Solid Films*, 2004, **464–465**, 368.
13 (*a*) N. Hamada, S.-I. Sawada and A. Oshiyama, *Phys. Rev. Lett*., 1992, **68**, 1579; (*b*) M. S. Dresselhaus, G. Dresselhaus and P. C. Eklund, *Science of Fullerenes and Carbon Nanotubes*, Academic Press Inc., San Diego, ch. 19, 1995.
14 I. W. Chiang, B. E. Brinson, A. Y. Huang, P. A. Willis, M. J. Bronikowski, J. L. Margrave, R. E. Smalley and R. H. Hauge, *J. Phys. Chem. B*, 2001, **105**, 8297.
15 (*a*) E. T. Mickelson, C. B. Huffman, A. G. Rinzler, R. E. Smalley, R. H. Hauge and J. L. Margrave, *Chem. Phys. Lett*., 1998, **296**, 188; (*b*) P. J. Boul, J. Liu, E. T. Mickelson, C. B. Huffman, L. M. Ericson, I. W. Chiang, K. A. Smith, D. T. Colbert, R. H. Hauge, J. L. Margrave and R. E. Smalley, *Chem. Phys. Lett*., 1999, **310**, 367; (*c*) M. Holzinger, O. Vostrowsky, F. H. Hirsch, M. Kappes, R. Weiss and F. Jellen, *Angew. Chem., Int. Ed*., 2001, **40**, 4002; (*d*) J. L. Bahr and J. L. Tour, *Chem. Mater*., 2001, **13**, 3823; (*e*) J. L. Bahr, J. Yang, D. V. Kosynkin, M. J. Bronikowski, R. E. Smalley and J. M. Tour, *J. Am. Chem. Soc*., 2001, **123**, 6536; (*f*) V. Georgakilas, K. Kordatos, M. Prato, D. M. Guldi, M. Holzinger and A. Hirsch, *J. Am. Chem. Soc*., 2002, **124**, 760; (*g*) P. Umek, J. W. Seo, K. Hernadi, A. Mrzel, P. Pechy, D. D. Mihailovic and L. Forr, *Chem. Mater*., 2003, **15**, 4751; (*h*) J. L. Stevens, A. Y. Huang, H. Peng, I. W. Chiang, V. N. Khabashesku and J. L. Margrave, *Nano Lett*., 2003, **3**, 331; (*i*) H. Peng, L. B. Alemany, J. L. Margrave and V. N. Khabashesku, *J. Am. Chem. Soc*., 2003, **125**, 15174; (*j*) H. Hu, B. Zhao, M. A. Hamon, K. Kamaras, M. E. Itkis and R. C. Haddon, *J. Am. Chem. Soc*., 2003, **125**, 14893; (*k*) S. Banerjee, M. G. C. Kahn and S. S. Wong, *Chem.-Eur. J*., 2003, **9**, 1898; (*l*) B. Zhao, H. Hu and R. C. Haddon, *Adv. Funct. Mater*., 2004, **14**, 71; (*m*) L. Zhang, V. U. Kiny, H. Pesng, J. Zhu, R. F. M. Lobo, J. L. Margrave and V. N. Khabashesku, *Chem. Mater*., 2004, **16**, 2055.
16 (*a*) M. A. Hamon, J. Chen, H. Hu, Y. Chen, M. E. Itkis, A. M. Rao, P. C. Eklund and R. C. Haddon, *Adv. Mater*., 1999, **11**, 834; (*b*) J. Zhang, H. Zou, Q. Qing, Y. Yang, Q. Li, Z. Liu, X. Guo and Z. Du, *J. Phys. Chem. B*, 2003, **107**, 3712.
17 J. L. Bahr and J. M. Tour, *J. Mater. Chem*., 2002, **12**, 1952.
18 (*a*) P. M. Ajayan, V. Ravikumar and J.-C. Charlier, *Phys. Rev. Lett*., 1998, **81**, 1437; (*b*) M. Igami, T. Nakanishi and T. Ando, *J. Phys. Soc. Jpn*., 1999, **68**, 716; (*c*) M. Igami, T. Nakanishi and T. Ando, *Physica B (Amsterdam)*, 2000, **284**, 1746; (*d*) A. V. Krasheninnikov and K. Nordlund, *Phys. Solid State*, 2002, **44**, 470; (*e*) J.-C. Charlier, *Acc. Chem. Res*., 2002, **35**, 1063; (*f*) A. V. Krasheninnikov and K. Nordlund, *J. Vac. Sci. Technol., B*, 2002, **20**, 728; (*g*) A. J. Lu and B. C. Pan, *Phys. Rev. Lett*., 2004, **92**, 105504; (*h*) V. V. Belavin, L. G. Bulusheva and A. V. Okotrub, *Int. J. Quantum Chem*., 2004, **96**, 239; (*i*) L. Valentini, F. Mercuri, I. Armentano, C. Cantalini, S. Picozzi, L. Lozzi, S. Santucci, A. Sgamellotti and J. M. Kenny, *Chem. Phys. Lett*., 2004, **387**, 356; (*j*) L. V. Liu, W. Q. Tian and Y. A. Wang, *J. Phys. Chem. B*, 2006, **110**, 1999.
19 (*a*) D. L. Carroll, Ph. Redlich, X. Blase, J.-C. Charlier, S. Curran, P. M. Ajayan, S. Roth and M. Rühle, *Phys. Rev. Lett*., 1998, **81**, 2332; (*b*) W. Han, Y. Bando, K. Kurashima and T. Sato, *Chem. Phys. Lett*., 1999, **299**, 368; (*c*) S. Peng and K. Cho, *Nano Lett*., 2003, **3**, 513; (*d*) M. Zhao, Y. Xia, J. Lewis and R. Zhang, *J. Appl. Phys*., 2003, **94**, 2398; (*e*) A. V. Nikulkina and P. N. D'yachkov, *Russ. J. Inorg. Chem*., 2004, **49**, 430.
20 (*a*) Ph. Lambin, A. A. Lucas and J. C. Charlier, *J. Phys. Chem. Solids*, 1997, **58**, 1833; (*b*) H. J. Choi, J. Ihm, S. G. Louie and M. L. Cohen, *Phys. Rev. Lett*., 2000, **84**, 2917; (*c*) M. B. Nardelli, J.-L. Fattebert, D. Orlikowski, C. Roland, Q. Zhao and J. Bernholc, *Carbon*, 2000, **38**, 1703; (*d*) H.-F. Hu, Y.-B. Li and H.-B. He, *Diamond Relat. Mater*., 2001, **10**, 1818; (*e*) L. G. Zhou and S. Q. Shi, *Carbon*, 2003, **41**, 579; (*f*) Y. Miyamoto, A. Rubio, S. Berber, M. Yoon and D. Tománek, *Phys. Rev. B*, 2004, **69**, 121413.
21 (*a*) D. E. Clemmer, J. M. Hunter, K. B. Shelimov and M. F. Jarrold, *Nature*, 1994, **372**, 248; (*b*) W. Branz, I. M. L. Billas, N. Malinowski, F. Tast, M. Heinebrodt and T. P. Martin, *J. Chem. Phys*., 1998, **109**, 3425; (*c*) J. M. Poblet, J. Muñoz, K. Winkler, M. Cancilla, A. Hayashi, C. B. Lebrilla and A. L. Balch, *Chem. Commun*., 1999, 493; (*d*) Q. Kong, Y. Shen, L. Zhao, J. Zhuang, S. Qian, Y. Li, Y. Lin and R. Cai, *J. Chem. Phys*., 2002, **116**, 128; (*e*) A. Hayashi, Y. Xie, J. M. Poblet, J. M. Campanera, C. B. Lebrilla and A. L. Balch, *J. Phys. Chem. A*, 2004, **108**, 2192.
22 (*a*) C. Ding, J. Yang, X. Cui and C. T. Chan, *J. Chem.Phys*., 1999, **111**, 8481; (*b*) I. M. L. Billas, C. Massobrio, M. Boero, M. Parrinello, W. Branz, F. Tast, N. Malinowski, M. Heinebrodt and T. P. Martin, *Comput. Mater. Sci*., 2000, **17**, 191.
23 A. De Vita, J.-Ch. Charlier, X. Blase and R. Car, *Appl. Phys. A*, 1999, **68**, 283.
24 R. Tamura and M. Tsukada, *Phys. Rev. B*, 1995, **52**, 6015.
25 (*a*) P. Hohenberg and W. Kohn, *Phys. Rev*., 1964, **136**, B864; (*b*) W. Kohn and L. J. Sham, *Phys. Rev*., 1965, **40**, A1133; (*c*) R. G. Parr and W. Yang, *Density-functional theory of atoms and molecules*, Oxford University Press, New York, 1989.
26 A. D. Becke, *Phys. Rev. A*, 1988, **38**, 3098.
27 (*a*) J. P. Perdew, J. A. Chevary, S. H. Vosko, K. A. Jackson, M. R. Pederson, D. J. Singh and C. Fiolhais, *Phys. Rev. B*, 1992, **46**, 6671; (*b*) J. P. Perdew, K. Burke and Y. Wang, *Phys. Rev. B*, 1996, **54**, 16533.
28 (*a*) R. Ditchfield, W. J. Hehre and J. A. Pople, *J. Chem. Phys*., 1971, **54**, 724; (*b*) W. J. Hehre, R. Ditchfield and J. A. Pople, *J. Chem. Phys*., 1972, **56**, 2257; (*c*) P. C. Hariharan and J. A. Pople, *Mol. Phys*., 1974, **27**, 209; (*d*) M. S. Gordon, *Chem. Phys. Lett*., 1980, **76**, 163.
29 P. J. Hay and W. R. Wadt, *J. Chem. Phys*., 1985, **82**, 299.
30 (*a*) Y. Sheng, D. G. Musaev, K. S. Reddy, F. E. McDonald and K. Morokuma, *J. Am. Chem. Soc*., 2002, **124**, 4149; (*b*) W. Q. Tian and Y. A. Wang, *J. Org. Chem*., 2004, **69**, 4299.

31 (*a*) A. D. Becke, *J. Chem. Phys*., 1993, **98**, 5648; (*b*) C. Lee, W. Yang and R. G. Parr, *Phys. Rev. B*, 1988, **37**, 785; (*c*) B. Miehlich, A. Savin, H. Stoll and H. Preuss, *Chem. Phys. Lett*., 1989, **157**, 200.
32 (*a*) A. E. Reed and F. Weinhold, *J. Chem. Phys*., 1983, **78**, 4066; (*b*) J. E. Carpenter, PhD thesis, University of Wisconsin, Madison, WI, 1987; (*c*) J. E. Carpenter and F. Weinhold, *J. Mol. Struct. (THEOCHEM)*, 1988, **169**, 41; (*d*) A. E. Reed, L. A. Curtiss and F. Weinhold, *Chem. Rev*., 1988, **88**, 899.
33 M. J. Frisch *et al*., *GAUSSIAN 03 (Revision B.05)*, Gaussian, Inc., Wallingford, CT, 2004.
34 T. Yumura, S. Bandow, K. Yoshizawa and S. Iijima, *J. Phys. Chem. B*, 2004, **108**, 11426.
35 G. Mpourmpakis, G. E. Froudakis, A. N. Andriotis and M. Menon, *Appl. Phys. Lett*., 2005, **87**, 193105.

Physical Chemistry Chemical Physics
RSC Publishing

- Journals
- Physical Chemistry Chemical Physics
- Contents List
- DOI: 10.1039/b604032m

- *Phys. Chem. Chem. Phys.*, 2006, **8**, 3528-3539
- DOI: 10.1039/b604032m
- Paper

Electronic properties and reactivity of Pt-doped carbon nanotubes†

Wei Quan Tian‡, Lei Vincent Liu and Yan Alexander Wang*
Department of Chemistry, University of British Columbia, Vancouver, BC V6T 1Z1, Canada. E-mail: yawang@chem.ubc.ca

Received 17th March 2006, Accepted 24th April 2006

First published on the web 19th May 2006

The structures of the (5,5) single-walled carbon nanotube (SWCNT) segments with hemispheric carbon cages capped at the ends (SWCNT rod) and the Pt-doped SWCNT rods have been studied within density functional theory. Our theoretical studies find that the hemispheric cages introduce localized states on the caps. The cap-Pt-doped SWCNT rods can be utilized as sensors because of the sensitivity of the doped Pt atom. The Pt-doped SWCNT rods can also be used as catalysts, where the doped Pt atom serves as the enhanced and localized active center on the SWCNT. The adsorptions of C_2H_4 and H_2 on the Pt atom in the Pt-doped SWCNT rods reveal different adsorption characteristics. The adsorption of C_2H_4 on the Pt atom in all of the three Pt-doped SWCNT rods studied (cap-end-doped, cap-doped, and wall-doped) is physisorption with the strongest interaction occurring in the middle of the sidewall of the SWCNT. On the other hand, the adsorption of H_2 on the Pt atom at the sidewall of the SWCNT is chemisorption resulting in the decomposition of H_2, and the adsorption of H_2 at the hemispheric caps is physisorption.

I. Introduction

Since the discovery of the single-walled carbon nanotube (SWCNT),[1] experimental and theoretical investigations on the chemical[2,3] and physical[4,5] properties of the SWCNT have been growing rapidly due to its potential applications[6] in molecular electronics,[7] chemical sensor,[8] vacuum electronic devices,[9] field emission flat panel display,[10] catalysis,[11] and optics.[12]

The SWCNT can be visualized as a roll of the graphite sheet and can be classified as metallic, narrow-gap and moderate-gap semiconducting nanotubes according to the wrapping vectors (*m*,*n*).[13] As shown in Scheme 1, nanotubes are characterized with a chiral vector (***AB*** = *ma*+*nb*) in which nanotubes are wrapped and a translation vector in which nanotubes elongate. If *n*–*m* = 3*q* (with integral *m*, *n*, and *q*), the nanotube is metallic. Otherwise, it is semiconducting with a band gap.[13b] There are further detailed classifications of nanotubes with respect to the conductance according to the "*n*–*m* rules".[13]

As one-dimensional (1-D) rolled graphite sheets, nanotubes display different electronic properties from those of planar graphite sheets and fullerenes: the electronic properties of nanotubes can be controlled by their diameters with different hybridization effects.[5a] For example, the pyramidization of nanotubes is different from fullerenes and there exists π-orbital misalignment between adjacent pairs of conjugated carbon atoms,[2a] which renders different reactivity of nanotubes from fullerenes and among nanotubes of various diameters.[2a,5e,14] Chemical reactions can take place on the sidewall of the nanotubes[15] or at the ends of the nanotubes.[15i,15k,16] In spite of numerous studies, the reactivity of the SWCNT is still not clear and deserves further investigation.[17]

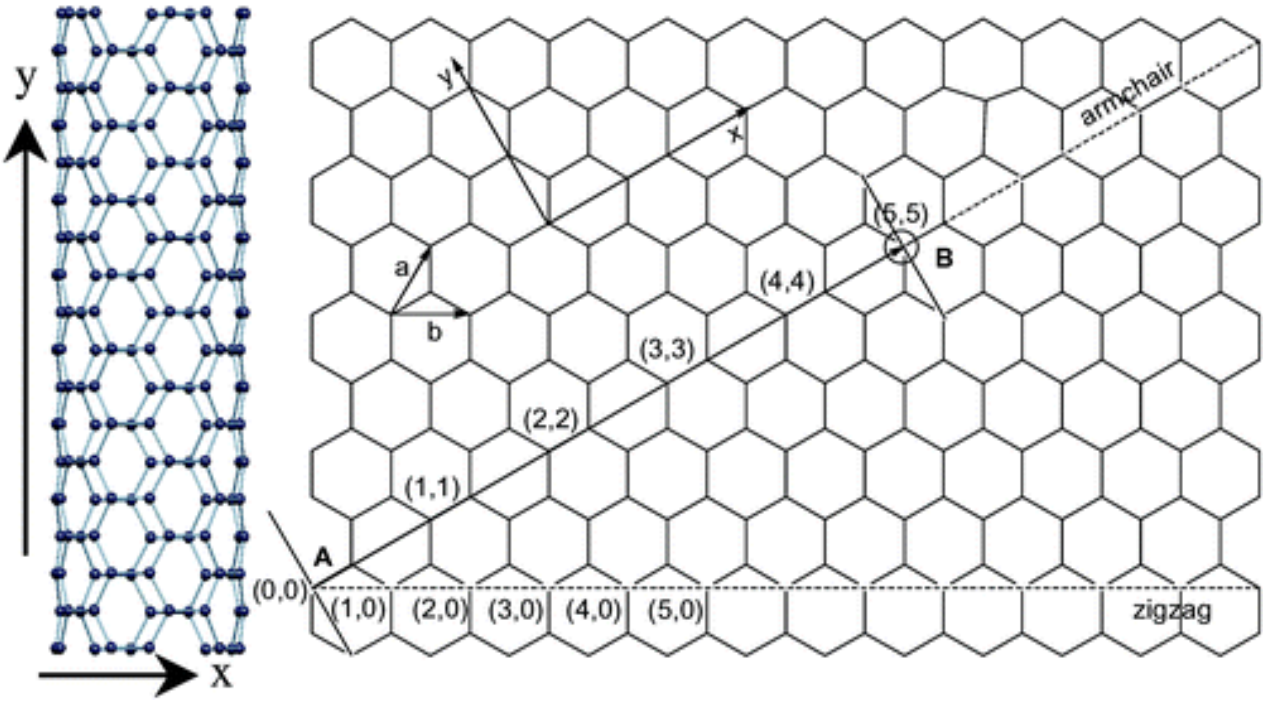

Scheme 1 Illustration of possible wrappings of the graphite sheet to the SWCNTs. Structure of the (5,5) SWCNT is shown on the left. The *x*-axis is the wrapping direction and the *y*-axis is the elongation direction. ***AB*** is the chiral vector.

Partial changes in the nanotube structure through vacancy,[18] doping with other elements (replacement of the carbon atoms on the SWCNT to produce the hetero SWCNT),[19] and distortion[20] can modify the

electronics and reactivity of the nanotubes to some degree.[18g,19c] It has been found that substituting a carbon atom by a metal atom in fullerenes[21] renders the metal atom as an active center in chemical reactions.[21e,22] As a pseudo 1-D system with tube structure, the SWCNT with defects and doping can serve as a catalyst for gas-phase and liquid-phase reactions: the reactants enter from one end of an open SWCNT, the reaction is catalyzed at the defect or doping sites of the SWCNT, and the products exit from the other end of the open SWCNT. A good understanding of the electronic structure of the perfect, defected, and doped SWCNTs helps to comprehend the reactivity of such SWCNTs and to utilize such SWCNTs in chemical reactions.

In this work, we will study the structures and reactivity of the hetero SWCNTs (HSWCNTs) to shed some light on the reactivity of such HSWCNTs and their possible applications. Unlike most main group element doped HSWCNTs,[19] the HSWCNTs we study here are the transition-metal doped (more specifically, precious-metal Pt doped) HSWCNTs.

II. Models and computational details

The model for the SWCNT is chosen to be the (5,5) armchair metallic SWCNT with two hemispheric caps, which are the half spheres of the fullerene. The open ends of the SWCNT were found to be active centers in many reactions, *e.g.* oxidation of the SWCNT,[16b] and the structure of the open ends goes through bond–distance reconstruction.[3i] No end-localized state has been found at energies near the Fermi surface for the open-end SWCNT.[3i] On the contrary, the caps in the capped nanorod were predicted to be important for the electronic properties of the nanorod[3d] and there exist electronic states localized on the caps[4a,23] because of the less stable pentagons,[24] despite that there is no significant contributions to the highest occupied molecular orbital (HOMO) and the lowest unoccupied molecular orbital (LUMO) of the nanorod from the caps.[3c] However, the differences in curvature and π bonding distinguish the chemical properties of fullerenes and the SWCNTs[2a] and thus divide the nanorod into at least two regions: the caps and the sidewall.

The structures of the (5,5) SWCNT rod and the Pt-doped (5,5) SWCNT rod with substitutions at the middle of the sidewall and at one of the end caps are studied with density functional theory (DFT).[25] Becke's exchange functional (B)[26] and Perdew's correlation functional (PW91)[27] based on the generalized gradient approximations are employed in structure optimization and property prediction. Pople's 6-31G[28] Gaussian basis set is used for carbon atoms and the relativistic 18-electron Los Alamos National Laboratory (LANL2DZ) effective core pseudopotential[29] with the basis set (3s3p2d) is used for the Pt atom. Because of its better predictive ability of relative energies,[30] the hybrid DFT method B3LYP[31] with the smaller LANL2MB[29] basis set is used for the geometry optimizations of the adsorptions of C_2H_4 and H_2 on the Pt-doped SWCNTs and the absorption energies are further refined by single-point energy calculations with the bigger LANL2DZ basis set. Partial charge analysis is performed with the natural bond orbitals (NBOs).[32] The geometries of all the Pt-doped nanorods are reoptimized with B3LYP/LNL2MB. The Gaussian 03[33] quantum chemical package is employed for all calculations in the present work.

III. Results and discussions

1. Perfect SWCNT rods

Fig. 1 and 2 display the geometries of the two (5,5) SWCNT rods, C_{170} and C_{180}, with D_{5h} and D_{5d} symmetries, and their density of states (DOS) and local density of states (LDOS), respectively. The DOS displays the overall electronic structure of a system, while the LDOS shows the electronic structure of a particular region and indicates the contribution of the atoms in that particular region to the overall DOS. The plots of the DOS and the LDOS above zero are for the discussion of the chemistry of the systems hereafter.

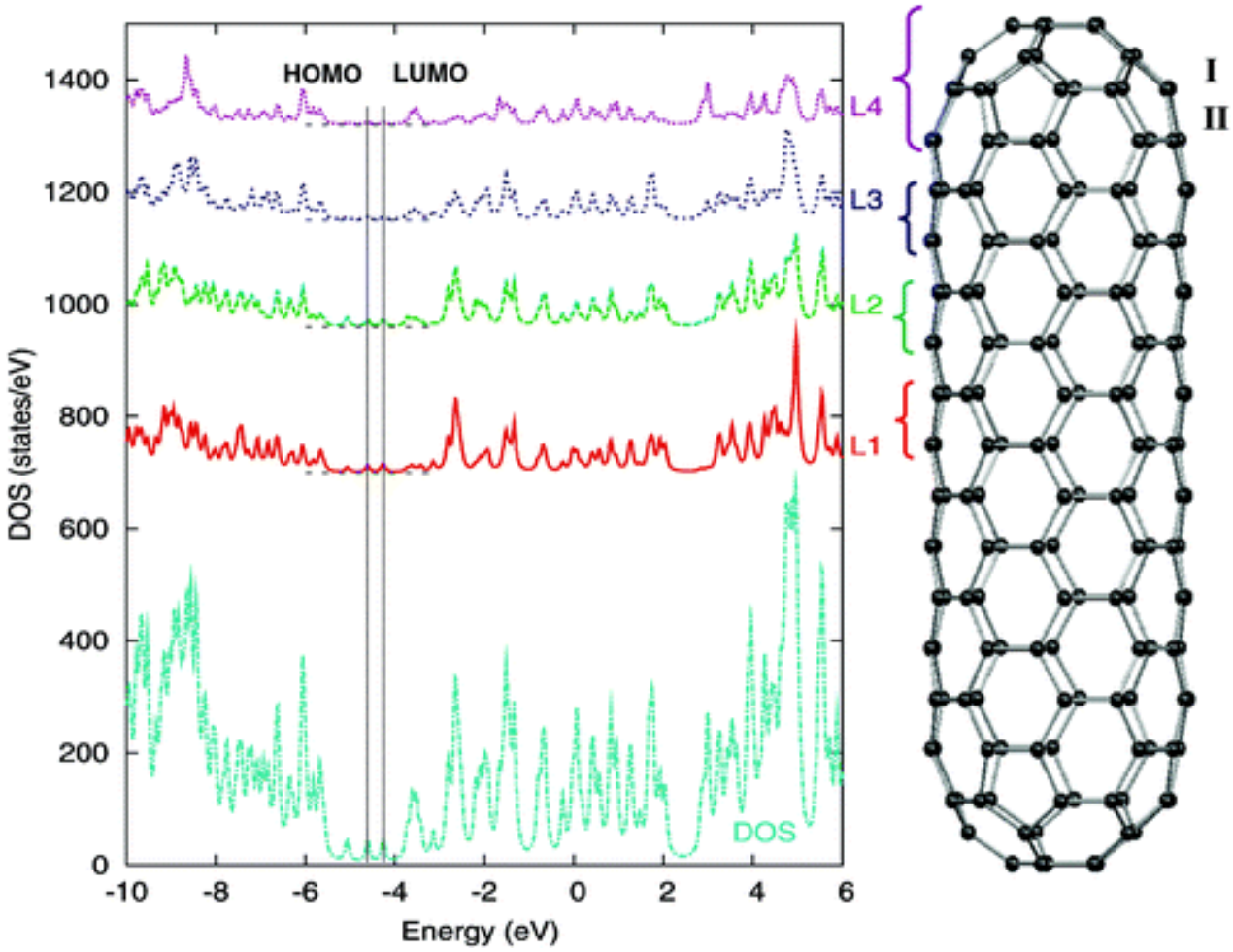

Fig. 1 Density of states and local density of states for nanorod C_{170} with the D_{5h} symmetry. HOMO is the highest occupied molecular orbital with orbital energy –4.61 eV, and LUMO is the lowest unoccupied molecular orbital with orbital energy –4.26 eV. L1, L2, L3, and L4 are the local densities of states for each specified layer of atoms of C_{170} as marked on the structure.

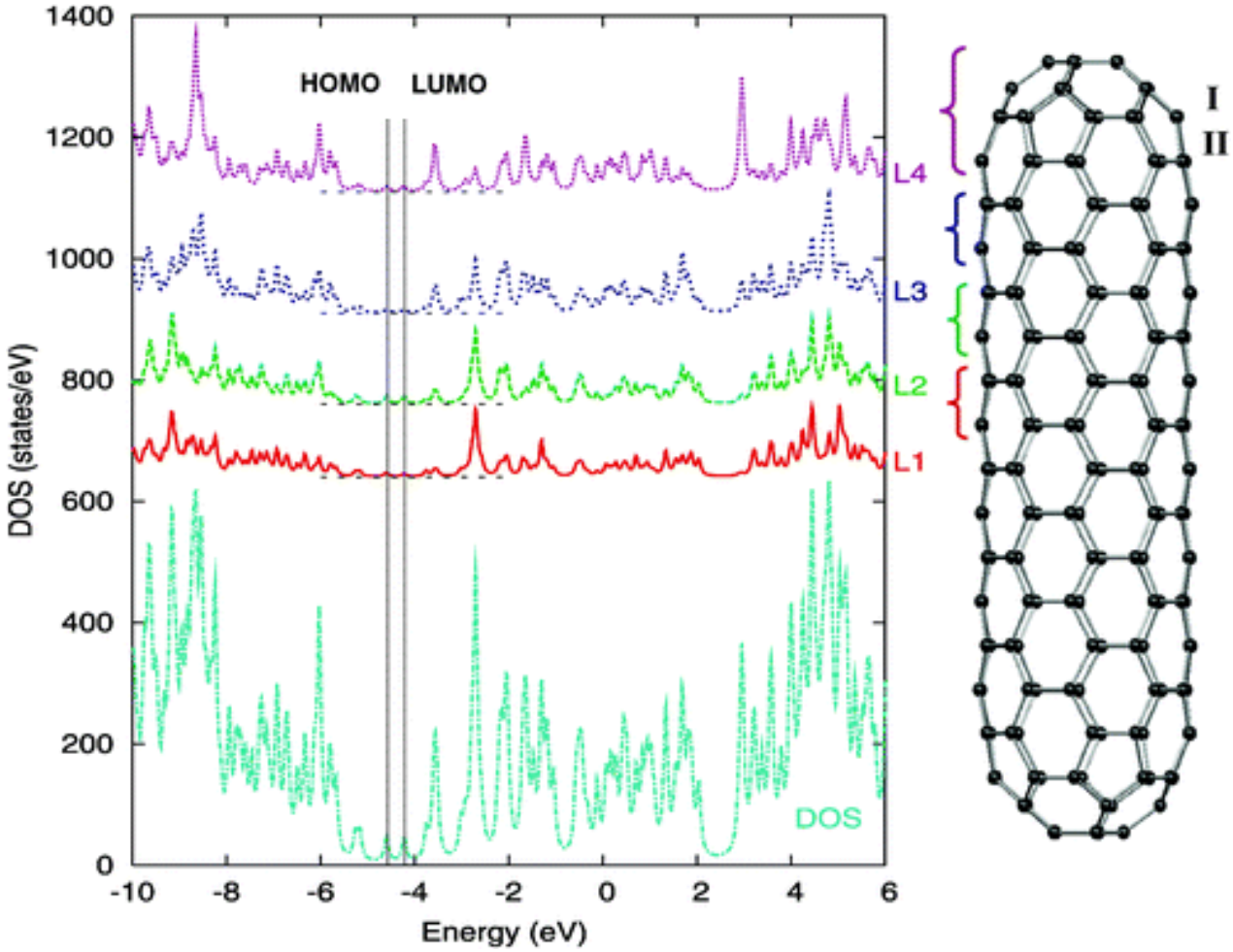

Fig. 2 Density of states and local density of states for nanorod C_{180} with the D_{5d} symmetry. HOMO is the highest occupied molecular orbital with orbital energy –4.60 eV, and LUMO is the lowest unoccupied molecular orbital with orbital energy –4.23 eV. L1, L2, L3, and L4 are the local densities of states for each specified layer of atoms of C_{180} as marked on the structure.

The similarity of the DOS and the LDOS of these two SWCNT rods is expected, since only one additional circular *cis*-polyene chain does not significantly change the electronic structure from C_{170} to C_{180}. Previous studies also found similarity in the HOMO–LUMO gaps of the (5,5) SWCNT rods, C_{170} and C_{180}.[3d] Fig. 1 and 2 also exhibit the LDOS of the *cis*-polyene chains in C_{170} and C_{180} along the SWCNT axis and the LDOS of the cap (a hemisphere of C_{60}). The shapes of the LDOS of different layers are similar at the frontier molecular orbital (MO) region, which indicates delocalization of the frontier MOs of the SWCNT rods. The contributions to the HOMO, the LUMO, and other occupied frontier MOs from the caps are not significant; the contributions to the HOMO and the LUMO of C_{170} and C_{180} are mainly from the sidewalls of the SWCNTs. The conspicuous contributions to the DOS from the LDOS of the cap lie about 1.0 eV below the HOMO and 0.5 eV above the LUMO, as indicated in Fig. 1 and 2.

The MOs give detailed information about the contributions of the LDOS from each layer to the DOS of the SWCNT rod. The occupied and unoccupied frontier MOs for the SWCNT rods C_{170} and C_{180} are plotted in Fig. 3 and 4, respectively. The highest four occupied MOs of C_{170} and C_{180} are π orbitals with

contributions from the sidewalls of the SWCNT rods and are delocalized on the sidewalls. The occupied MOs with major contribution from the caps lie about 1 eV below the HOMO, similar to the picture manifested by the LDOS of the cap in Fig. 1 and 2. The HOMO and the LUMO have sole contributions from the sidewall of the SWCNT. The lowest two unoccupied MOs of C_{170} and C_{180} are delocalized π orbitals of the sidewalls of the SWCNTs and are followed by four (two two-fold degenerate) localized MOs on the caps. The patterns of the HOMO and the LUMO in C_{170} are different from their counterparts in C_{180}. Such a pattern change was observed for shorter SWCNT rods before.[3c]

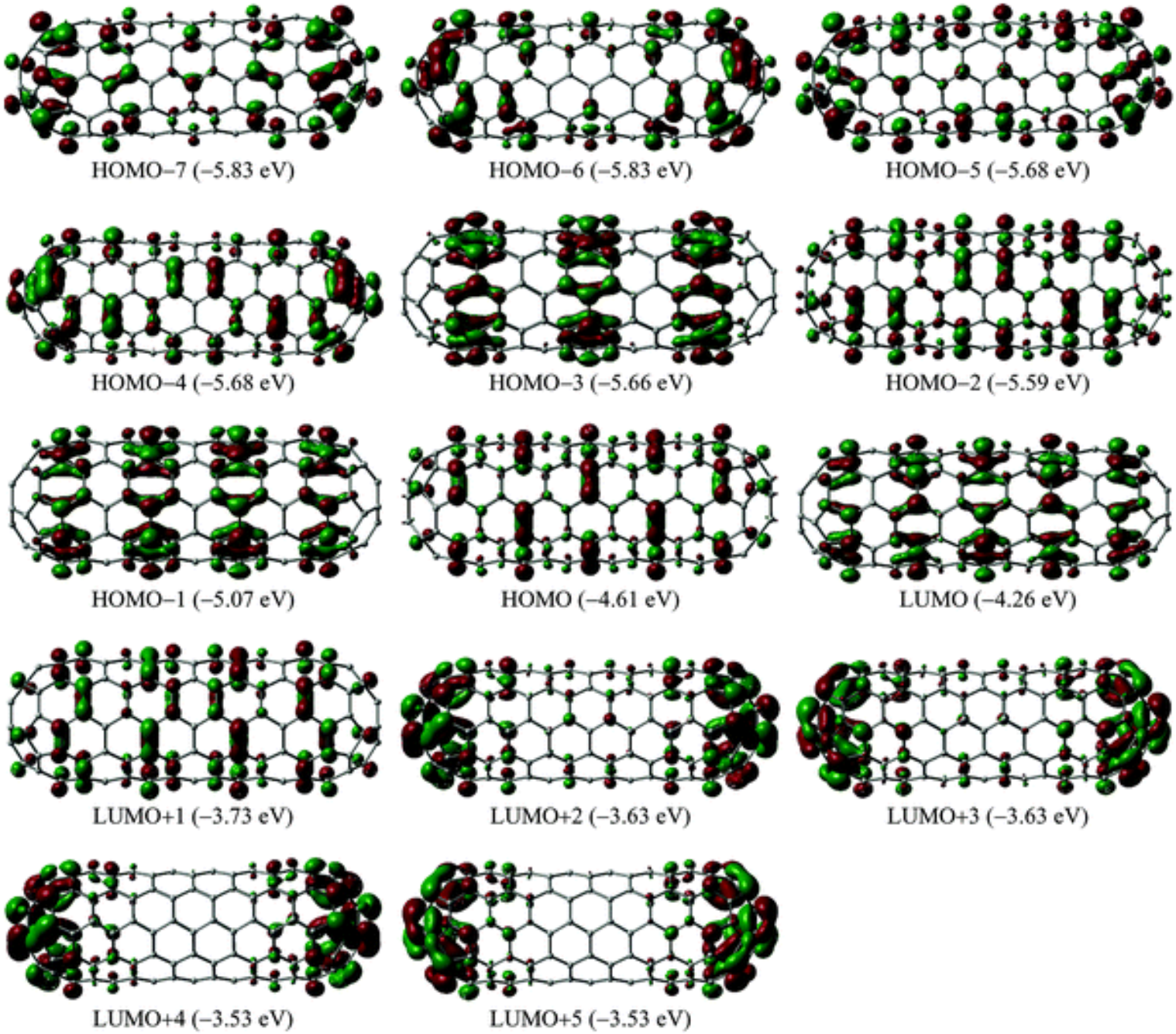

Fig. 3 Frontier orbitals of nanorod C_{170} with the D_{5h} symmetry. HOMO–*n* (*p* eV) is the *n*th orbital below the HOMO with orbital energy *p* eV. LUMO+*m* (*q* eV) is the *m*th orbital above the LUMO with orbital energy *q* eV.

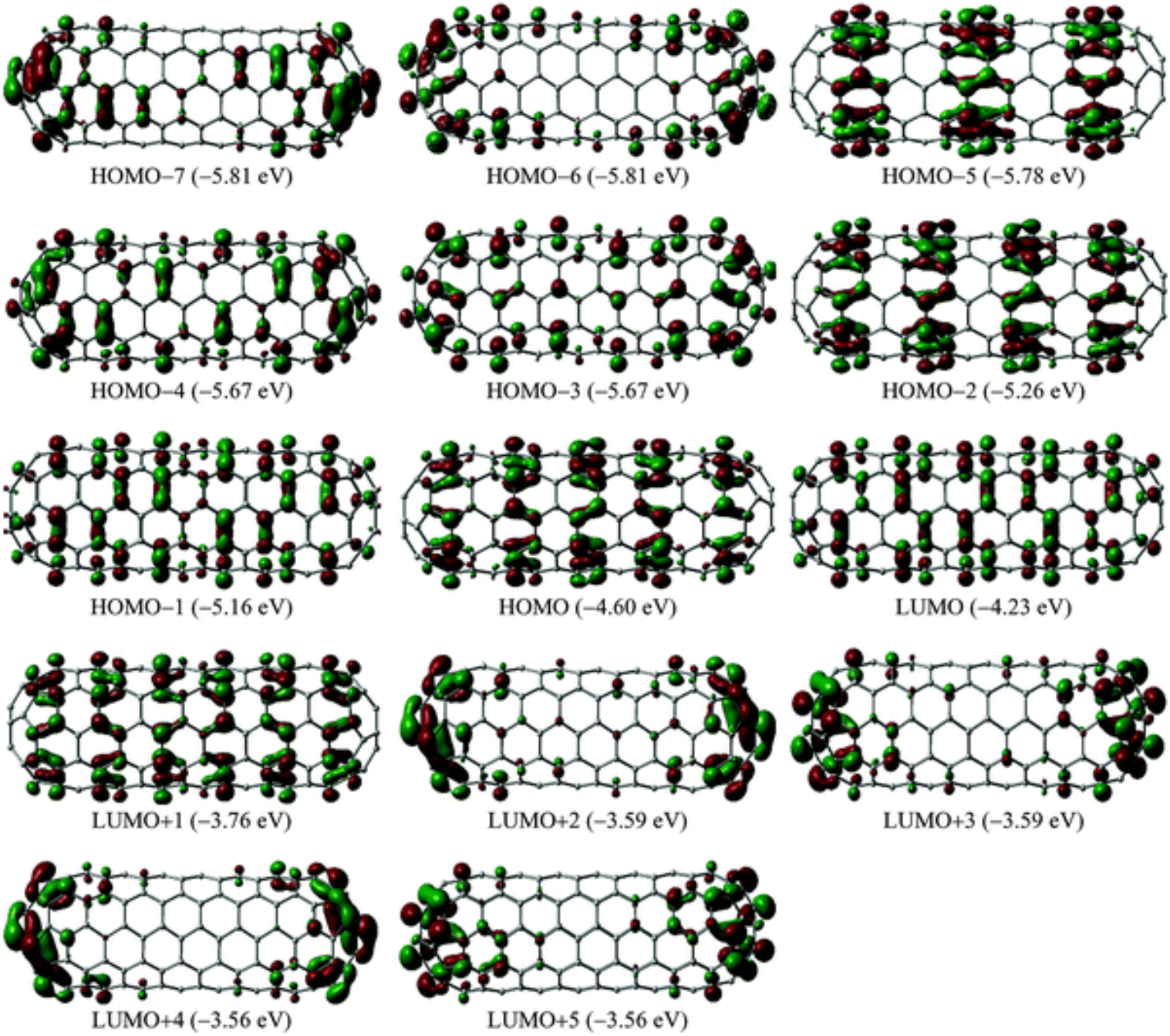

Fig. 4 Frontier orbitals of nanorod C_{180} with the D_{5d} symmetry. HOMO–*n* (*p* eV) is the *n*th orbital below the HOMO with orbital energy *p* eV. LUMO+*m* (*q* eV) is the *m*th orbital above the LUMO with orbital energy *q* eV.

From the MOs, one can infer that, when reacting with strong electron acceptors, the SWCNT rods C_{170} and C_{180} will donate electrons from the sidewalls of the SWCNTs to the electron acceptors. When C_{170} and C_{180} accept electrons, the first four electrons will go to the middle of the sidewalls of the SWCNTs, and any extra (up to eight) electrons will go to the caps. From the frontier occupied MOs of C_{170} and C_{180}, one cannot see clearly the separation of the electronic structure of the caps from the sidewall of the SWCNT, though there exists some gradual geometric change from the caps to the sidewall.[34] The delocalized MOs on the sidewall of the SWCNT rods extend to the ridge of the pentagons of the caps. The pentagon regions have 6–6 (between two hexagons) and 6–5 (between a hexagon and a pentagon) CC bond alternation, similar to that in C_{60}. From the MOs of C_{170} and C_{180}, one can infer that the

electronic structure on the caps is localized and the geometric (topological) role of the caps can be the dominant factor for determining the electronic properties of the SWCNT rods.[34]

The atoms on the last layer of L4 (II in Fig. 1 and 2) have the largest negative charge in C_{180} and a large negative charge in C_{170}. In chemical reactions, this layer is reactive toward electron acceptors and can be treated as a bridge between the sidewall and the cap of a SWCNT rod. The middle layers of the sidewall of the SWCNT rod have a positive charge.

For C_{170}, the vertical ionization potential (IP) and electron affinity (EA) are 5.86 and 2.89 eV, respectively.

Due to the similarity of the electronic and geometric structures of C_{170} and C_{180}, we will focus on C_{170} and its doping derivatives for the rest of the investigation.

2. Pt-doped SWCNT rods

For C_{170}, NBO partial charge analysis indicates that the five atoms connecting to the top pentagon of the cap have the largest negative charges and the atoms of the next layer (I in Fig. 1) have the largest positive charge. Thus, the caps can be chemical reaction centers. Substitution of the carbon atoms in the cap by other elements will change the chemical selectivity and sensitivity of the SWCNT rod in catalytic reactions. Replacing one carbon atom with a Pt atom in the end pentagon, in the next layer, or on the sidewall of C_{170} results in three Pt-doped SWCNT rods: the cap-end-doped C_{169}Pt(ce), the cap-doped C_{169}Pt(c), and the wall-doped C_{169}Pt(w), as shown in Fig. 5, 6, and 7. Single-point calculations at the BPW91/6-31G level of theory predict that C_{169}Pt(ce) is the most stable nanorod: the total energies of C_{169}Pt(c) and C_{169}Pt(w) are 0.8 and 17.9 kcal mol^{-1} higher, respectively. Evidently, the cap-doped SWCNTs are more stable than the wall-doped SWCNT, because of the relaxation of the constraint on the cap through doping. The total energy of the triplet electronic state of the Pt-doped nanorod is found to be higher than that of the singlet, *i.e.* the ground state of the Pt-doped nanorod is singlet.

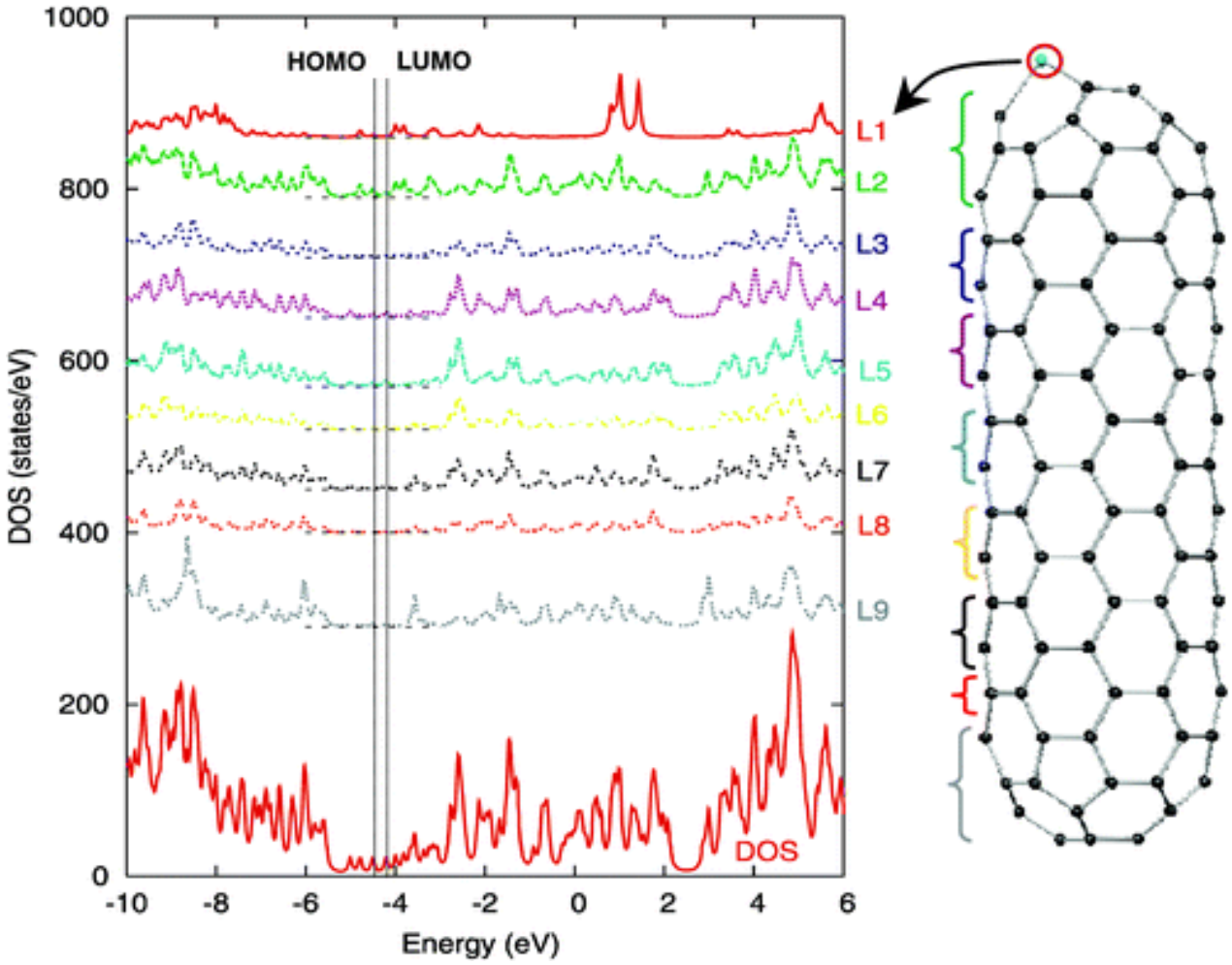

Fig. 5 Density of states and local density of states for the Pt cap-end-doped nanorod $C_{169}Pt(ce)$ with the C_s symmetry. HOMO is the highest occupied molecular orbital with orbital energy –4.51 eV, and LUMO is the lowest unoccupied molecular orbital with orbital energy –4.21 eV. L1, L2, L3, L4, L5, L6, L7, L8, and L9 are the local density of states for each specified layer of atoms of $C_{169}Pt(ce)$ as marked on the structure.

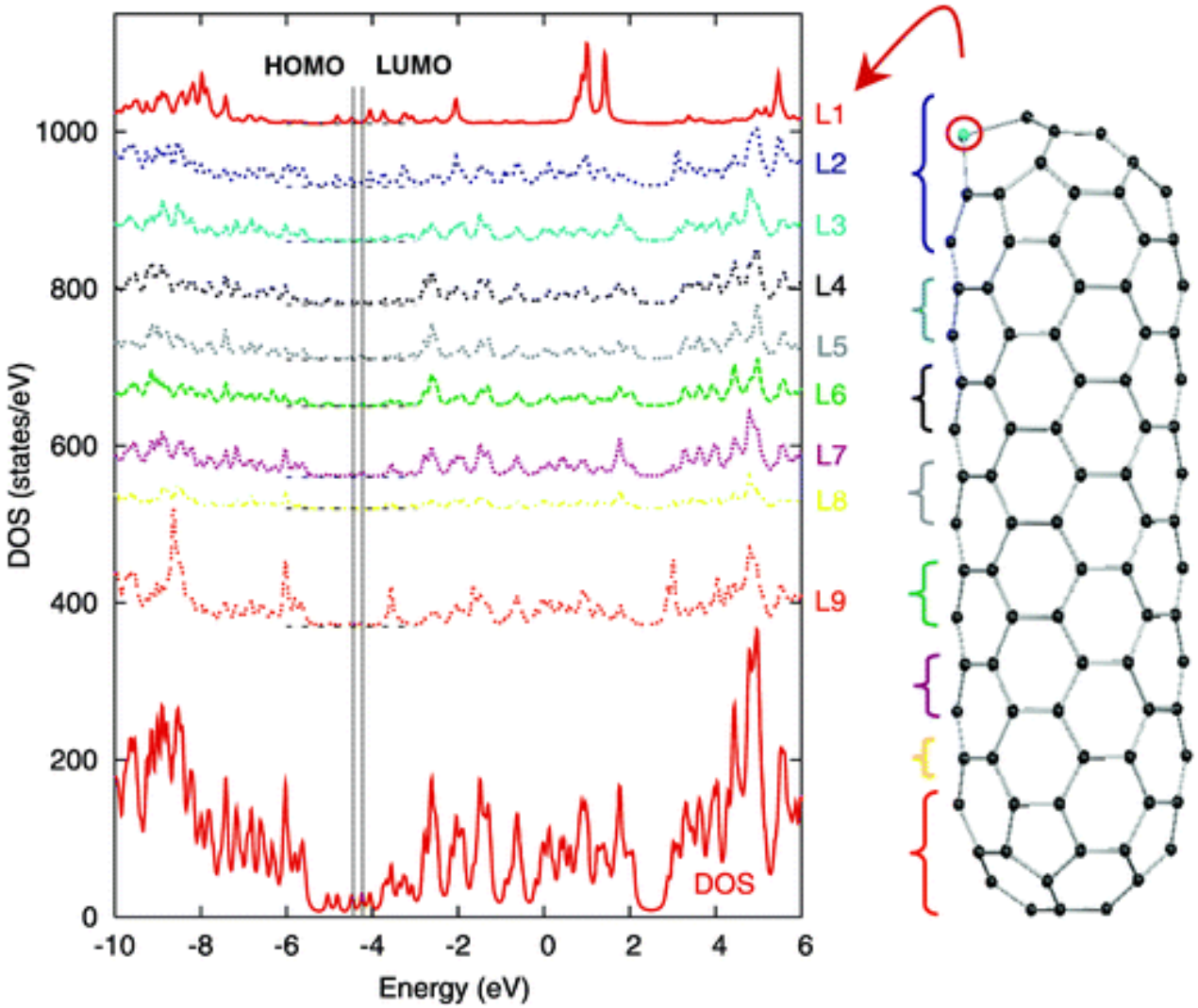

Fig. 6 Density of states and local density of states for the Pt cap-doped nanorod $C_{169}Pt$ (c) with the C_s symmetry. HOMO is the highest occupied molecular orbital with orbital energy –4.48 eV, and LUMO is the lowest unoccupied molecular orbital with orbital energy –4.25 eV. L1, L2, L3, L4, L5, L6, L7, L8, and L9 are the local density of states for each specified layer of atoms of $C_{169}Pt$(c) as marked on the structure.

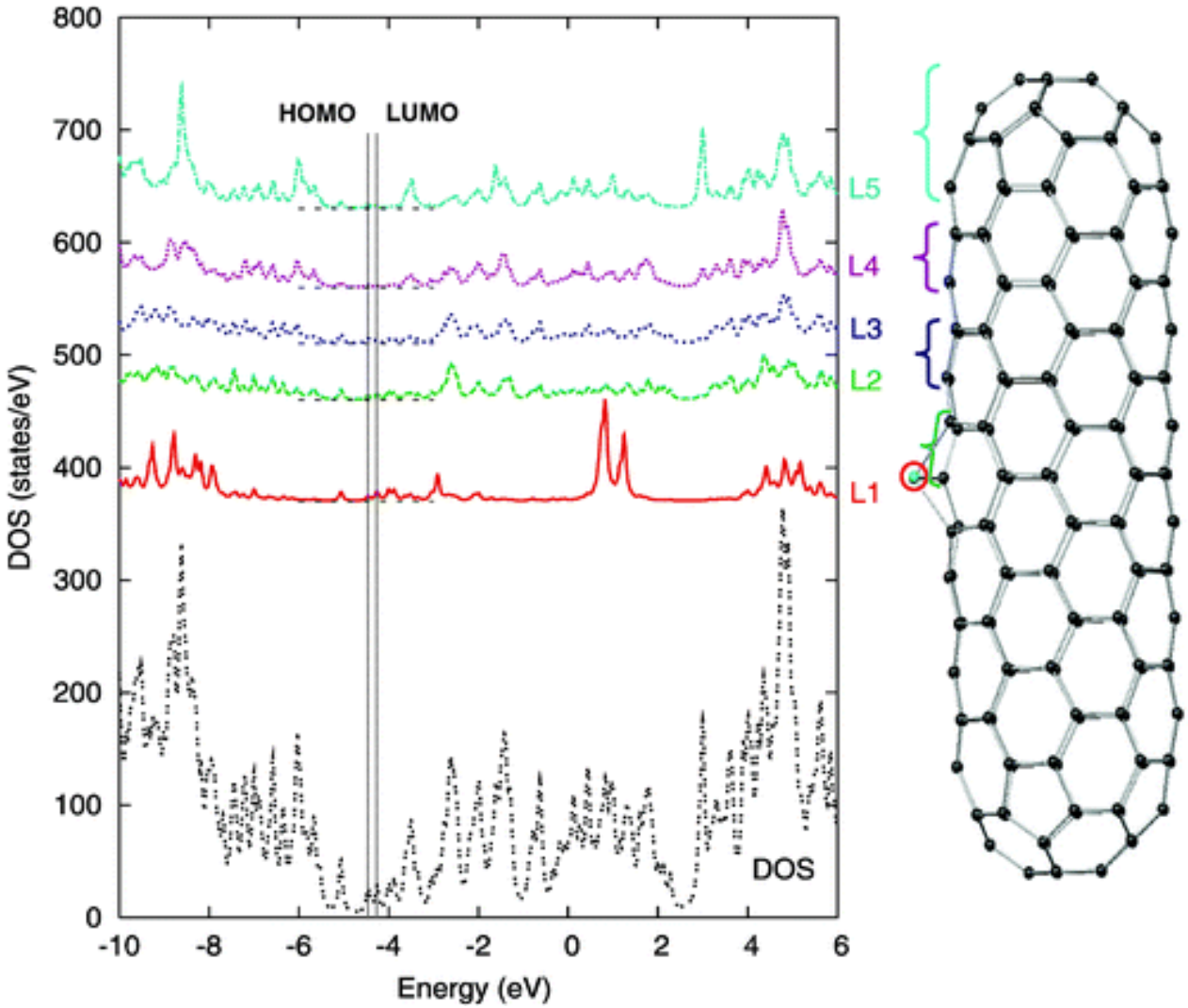

Fig. 7 Density of states and local density of states for the Pt wall-doped nanorod $C_{169}Pt$ (w) with the C_s symmetry. HOMO is the highest occupied molecular orbital with orbital energy –4.46 eV, and LUMO is the lowest unoccupied molecular orbital with orbital energy –4.26 eV. L1, L2, L3, L4, and L5 are the local densities of states for each specified layer of atoms of $C_{169}Pt$(w) as marked on the structure.

2.A. Cap-end-doped $C_{169}Pt$(ce). Fig. 5 and 8 display the structure, the DOS, the LDOS, and the frontier MOs of $C_{169}Pt$(ce). The Pt–C bond distances at the cap end are 2.01 Å and the other Pt–C bond distances are 1.96 Å. Clearly, the Pt atom points outwards along the translation direction of the SWCNT. The distortion of the SWCNT rod due to the Pt-doping is localized on the pentagons and hexagons around Pt. The overall DOS of $C_{169}Pt$(ce) is similar to that of C_{170} with the D_{5h} symmetry. The doping of Pt produces more peaks in the DOS in the frontier MO region due to the introduction of the Pt 5d orbitals and the induced electronic structure change in the doped cap. The LDOS of L1 and L2 in Fig. 5 clearly indicates such changes. L1 (the LDOS of Pt) in Fig. 5 manifests the contribution of Pt to the DOS of $C_{169}Pt$(ce). The LDOS of the remaining layers in Fig. 5 are similar to one another.

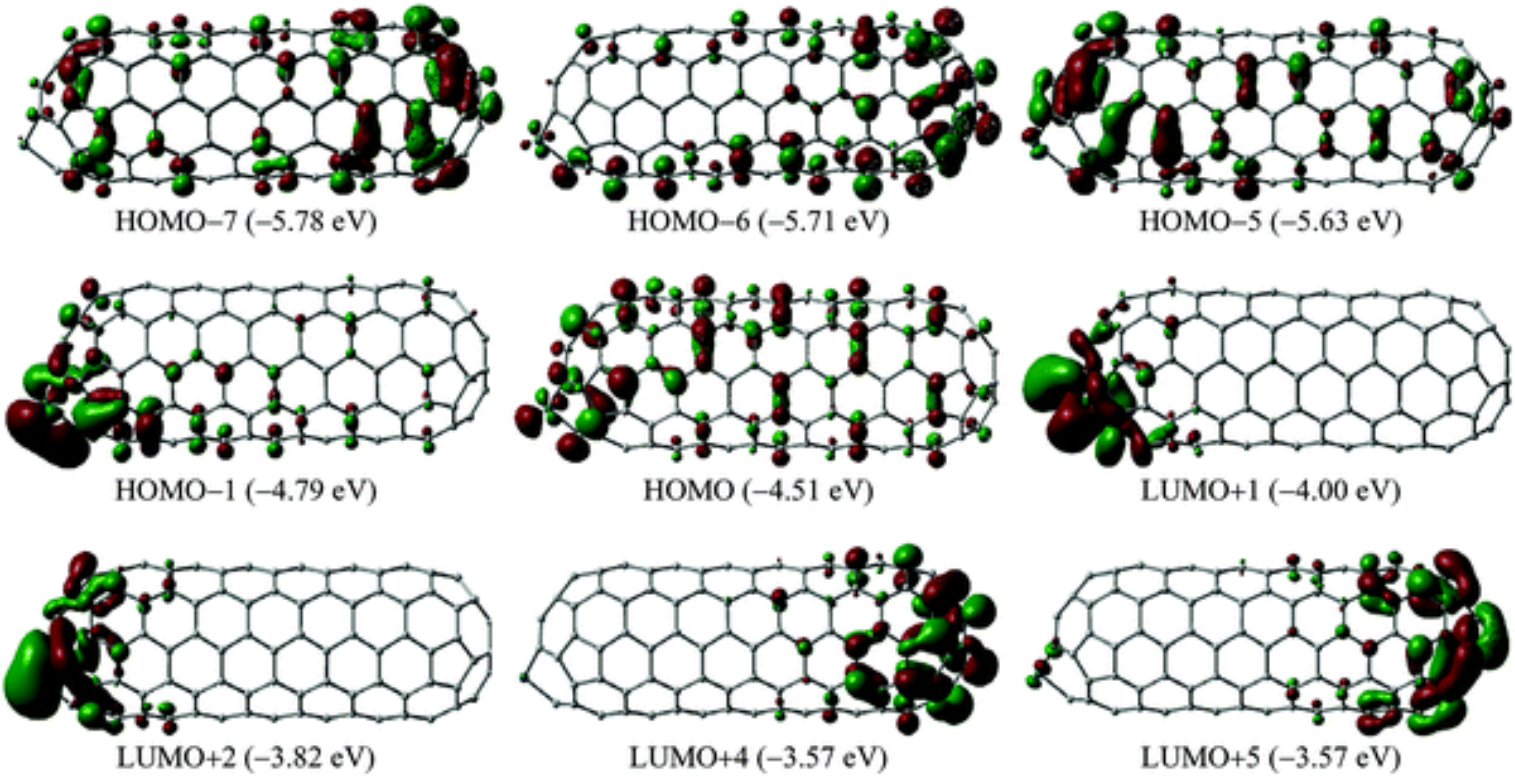

Fig. 8 Relevant frontier orbitals of the Pt cap-end-doped nanorod $C_{169}Pt(ce)$ with the C_s symmetry. HOMO–*n* (*p* eV) is the *n*th orbital below the HOMO with orbital energy *p* eV. LUMO+*m* (*q* eV) is the *m*th orbital above the LUMO with orbital energy *q* eV.

The frontier MOs in Fig. 8 reveal details of the electronic structure of $C_{169}Pt(ce)$. The HOMO of $C_{169}Pt(ce)$ is similar to that of C_{170}, except for the significant contributions from Pt and its neighboring carbon atoms in $C_{169}Pt(ce)$. The effect of Pt on the electronic structure of $C_{169}Pt(ce)$ is also reflected in several other occupied MOs: the HOMO–1, the HOMO–5, the HOMO–6, and the HOMO–7. The HOMO–1 has some major contributions from the Pt 5d orbitals, which form d-p π bonds with the carbon atoms in the next layer. The geometric distortion in $C_{169}Pt(ce)$ induces single and double CC bond alteration around Pt, which is reflected in the strong π bonding around the doped cap in the HOMO–5. The symmetry of the π bonds in the HOMO–7, the HOMO–6, and the HOMO–5 (corresponding to the HOMO–7, the HOMO–6, and the HOMO–5 in C_{170}) is destroyed in $C_{169}Pt(ce)$, resulting in concentrated π bonding on one end cap, as clearly shown in Fig. 8. The LUMO of $C_{169}Pt(ce)$ is very similar to that of C_{170}. The next two unoccupied MOs, the LUMO+1 and the LUMO+2, of $C_{169}Pt(ce)$ are mainly from the 5d orbitals of Pt, and the contribution to these two unoccupied MOs from the undoped cap diminishes. According to the MOs of $C_{169}Pt(ce)$, it is quite clear that the reactive center in $C_{169}Pt(ce)$ is around the location of Pt. The Pt atom can donate electrons to electron acceptors and its empty 5d orbitals can accept electrons from electron donors, *e.g.* in reaction with gases like H_2, C_2H_4, CO, NH_3, NO, *etc*. NBO partial charge analysis indicates that Pt transfers about 0.80 electrons (0.40 electrons from 6s and 0.40 electrons from 5d) to nearby carbons: the electronic configuration of the Pt atom is essentially $[core]5d^{8.60}6s^{0.60}$. The carbon atom connecting to Pt in the second layer from the doped cap end has the largest negative charge, –0.22.

The vertical IP and EA of $C_{169}Pt(ce)$ are 5.45 and 3.40 eV, respectively.

2.B. Cap-doped $C_{169}Pt(c)$. Fig. 6 shows that the DOS and the LDOS of each layer of atoms of $C_{169}Pt$ (c) are very similar to those of $C_{169}Pt$(ce). The structure of $C_{169}Pt$(c) is also similar to that of $C_{169}Pt$(ce), except for the region around Pt. The Pt–C bond distance between Pt and the carbon atom in the top pentagon is 1.97 Å; the other two equivalent Pt–C bond distances are 2.00 Å. The long Pt–C bonds make the carbon atom of the top pentagon connected to Pt slightly point out of the pentagon, as shown in Fig. 6. The frontier MOs of $C_{169}Pt$(c), as shown in Fig. 9, are very similar to those of $C_{169}Pt$(ce) in Fig. 8. The noticeable difference is that Pt contributes to the HOMO of $C_{169}Pt$(c) more than it does in $C_{169}Pt$ (ce), which will enhance the reactivity of Pt in $C_{169}Pt$(c). The electronic configuration of the Pt atom is essentially [core]$5d^{8.63}6s^{0.60}$. The partial charge of Pt is 0.77 and the carbon atom connecting to Pt in the top pentagon has the largest negative partial charge, –0.25. The vertical IP and EA of $C_{169}Pt$(c) are 5.49 and 3.21 eV, respectively.

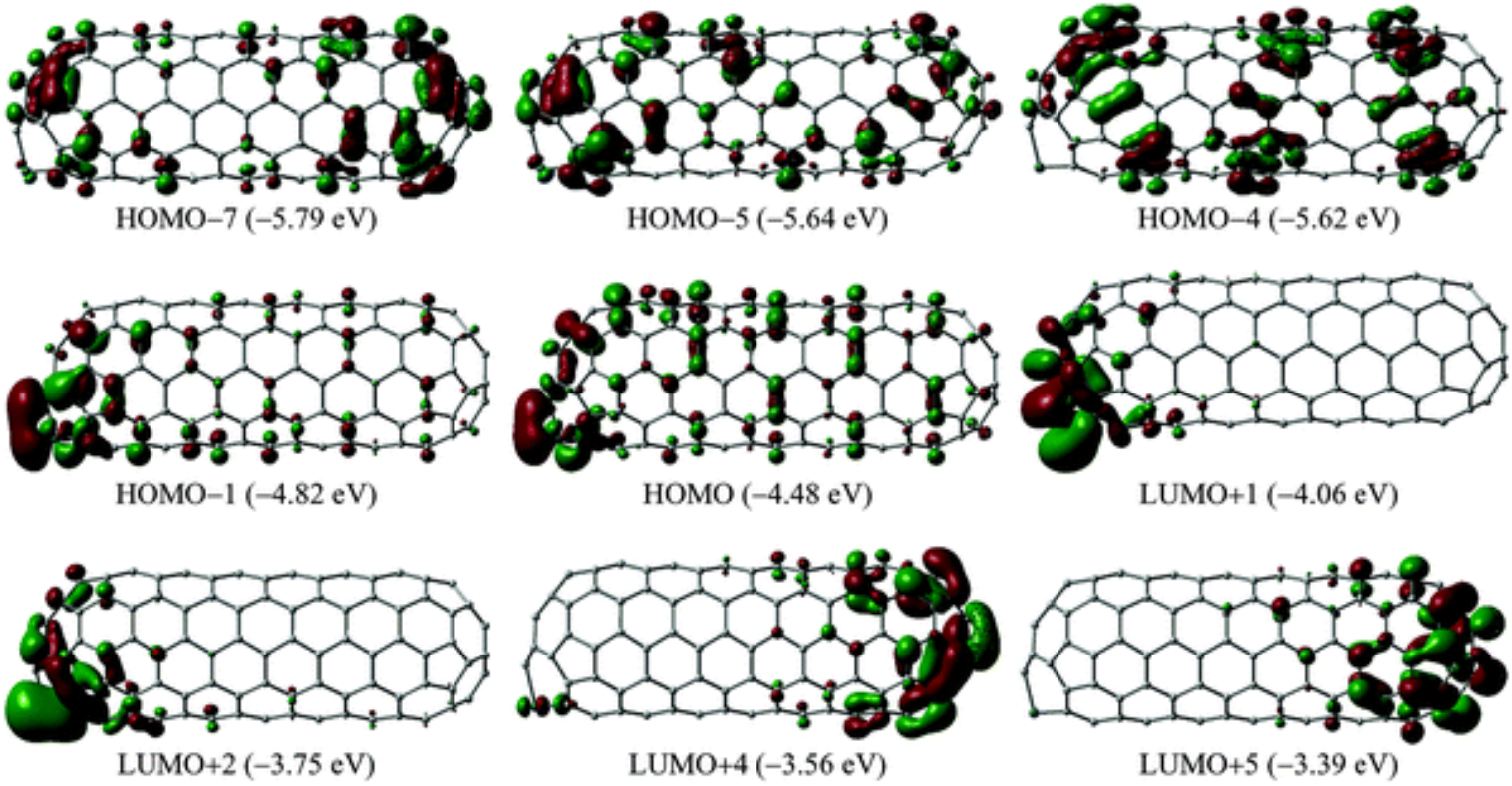

Fig. 9 Frontier orbitals of the Pt cap-doped nanorod $C_{169}Pt$(c) with the C_s symmetry. HOMO–*n* (*p* eV) is the *n*th orbital below the HOMO with orbital energy *p* eV. LUMO+*m* (*q* eV) is the *m*th orbital above the LUMO with orbital energy *q* eV.

2.C. Wall-doped $C_{169}Pt(w)$. Fig. 7 and 10 display the DOS, the LDOS of each layer, and the frontier MOs of $C_{169}Pt$(w). The DOS of $C_{169}Pt$(w) around the frontier MO region is different from those of $C_{169}Pt$ (ce) and $C_{169}Pt$(c): the contribution to the DOS at the frontier MO region from Pt has noticeably increased in $C_{169}Pt$(w). The LDOS of Pt indicates that Pt contributes significantly to the DOS at the frontier MO region in $C_{169}Pt$(w). The introduction of Pt on the sidewall of the SWCNT also drastically changes the LDOS of its neighboring carbon layers, which can be vividly demonstrated by the comparison of the LDOS of L2 and L3 in Fig. 7 with L1 and L2 of C_{170} in Fig. 1. The LDOS contribution from each layer is also depicted by the frontier MOs, as shown in Fig. 10. From the HOMO–1 to the LUMO+3, Pt has significant contributions to each MO. The HOMO–LUMO gap (0.20 eV) of

$C_{169}Pt(w)$ is smaller than those of C_{170} (0.35 eV), $C_{169}Pt(ce)$ (0.30 eV), and $C_{169}Pt(c)$ (0.23 eV). In chemical reactions, Pt will serve as various catalytic centers with flexible oxidation states capable of accepting and donating electrons. The electronic configuration of Pt is essentially [core]$5d^{8.63}6s^{0.54}$. The partial charge of Pt is 0.83. The partial charge of the carbon atom connecting to Pt in the symmetric plane is –0.18, where the Pt–C bond distance is 2.01 Å. The partial charges of the other two equivalent carbon atoms connecting to Pt are –0.10, and the two equivalent Pt–C bond distances are 1.95 Å. The vertical IP and EA of $C_{169}Pt(w)$ are 5.44 and 3.28 eV, respectively.

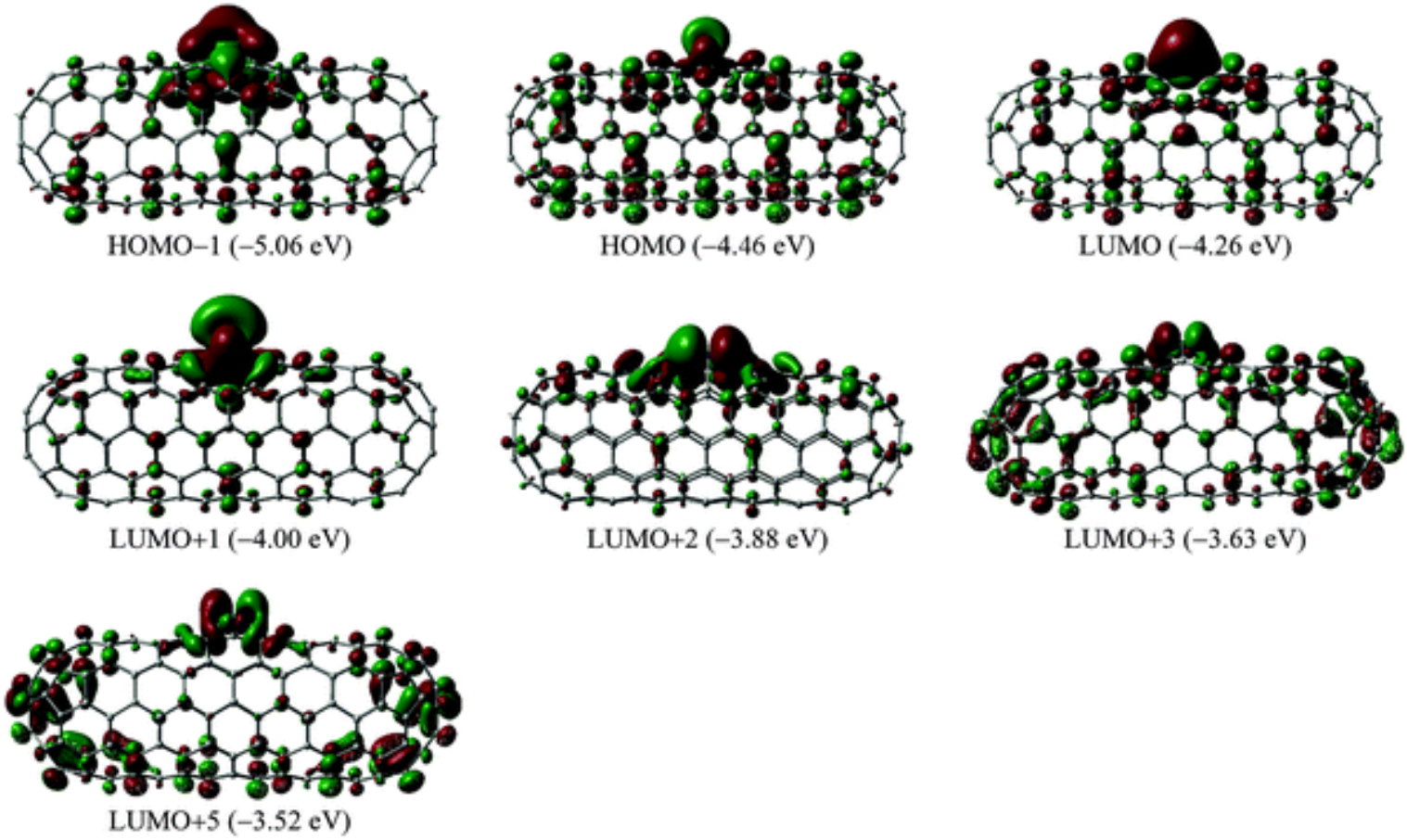

Fig. 10 Relevant frontier orbitals of the Pt wall-doped nanorod $C_{169}Pt(w)$ with the C_s symmetry. HOMO–*n* (*p* eV) is the *n*th orbital below the HOMO with orbital energy *p* eV. LUMO+*m* (*q* eV) is the *m*th orbital above the LUMO with orbital energy *q* eV.

3. Adsorptions of C_2H_4 and H_2 on $C_{169}Pt$

From the EAs and IPs of C_{170} and the three Pt-doped nanorods, one can see that the doping of Pt enhances both the electron accepting and donating capacities of the doped nanorod. Thus, the doping of Pt certainly changes the chemical reactivity and regioselectivity of the SWCNT and broadens the field of application of the SWCNT rods in such areas as gas sensors.[35] Present studies have found that the change of structure and reactivity through the doping of Pt in the SWCNT is localized at the doping site. To reveal the different reactivity of the Pt-doped SWCNTs, we are now studying adsorptions of C_2H_4 and H_2 on the Pt atom of the three Pt-doped SWCNTs. The relative stability of the Pt-doped SWCNTs and the adsorption energies of C_2H_4 and H_2 on the Pt-doped SWCNTs are collected in Table 1.

Table 1 The relative stabilities of the Pt-doped nanorods and the adsorption energies of C_2H_4 and H_2 on the Pt-doped nanorods. The minus sign indicates the release of the heat of formation upon the adsorption. All energies are in kcal mol^{-1}

Adsorbate	Level of theory	$C_{169}Pt$(ce)	$C_{169}Pt$(c)	$C_{169}Pt$(w)
None	BPW/6-31G	0.0	0.8	17.9
	B3LYP/Lanl2mb	0.0	2.4	28.6
	B3LYP/Lanl2dz	0.0	3.3	26.3
C_2H_4	B3LYP/Lanl2mb	–22.4	–23.5	–19.2
	B3LYP/Lanl2dz	–20.6	–22.2	–14.7
H_2	B3LYP/Lanl2mb	–2.1	–2.3	–10.7
	B3LYP/Lanl2dz	–2.8	–3.0	–10.9

As can be seen from the bond distances at the adsorption site in Fig. 11, there is no significant structural change at the Pt-doped region for the adsorption of H_2 on the two cap-doped SWCNTs, as exemplified by the Pt–C bond distances. These two cases are physisorptions according to the H–H bond distance and the distances between H_2 and the SWCNT shown in Fig. 11 and the adsorption energies in Table 1. On the other hand, the adsorption of H_2 on the Pt atom in the middle of the nanorod $C_{169}Pt$(w) is a chemical one. Obviously, the H–H bond is broken and the two hydrogen atoms form chemical bonds with Pt with bond lengths of *ca.* 1.70 Å. The distance between the two hydrogen atoms is 2.29 Å. This chemisorption releases about 10.0 kcal mol^{-1} energy, which is nearly five times the energy (about 2.0 ~ 3.0 kcal mol^{-1}) released by the adsorption of H_2 on the Pt atom at the end cape of the SWCNT rods. The interaction between H_2 and Pt in the two physisorptions is mainly the electron transfer from the bonding orbital of H_2 to the empty 5d orbital of Pt, as indicated by the MOs in Fig. 12. Though the two hydrogen atoms in the adsorption on $C_{169}Pt$(w) are separated, the interaction between these two hydrogen atoms remains strong, as revealed by the MO overlaps between them (Fig. 12).

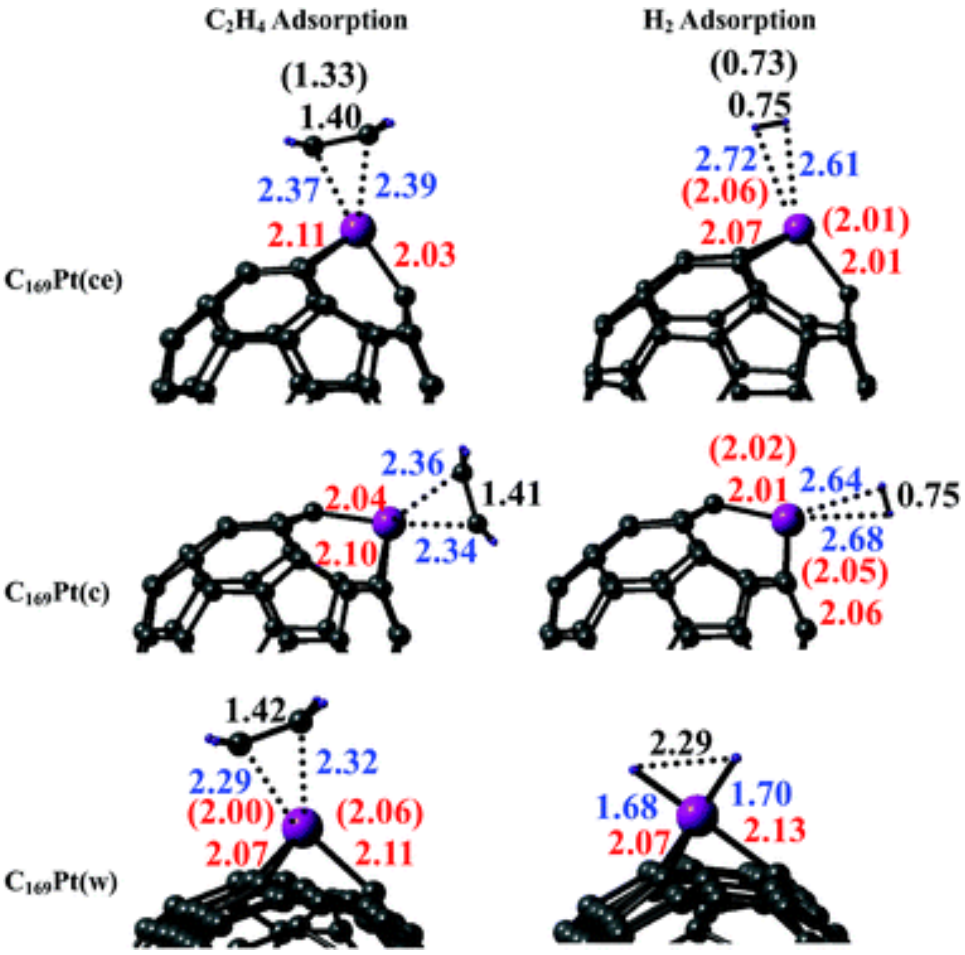

Fig. 11 The relevant bond distances (in Å) of the adsorptions of C_2H_4 and H_2 on the Pt atom in the Pt-doped nanorods ($C_{169}Pt$). The Pt atom is the big ball. The C=C bond distances in the C_2H_4 adsorption are about 1.4 Å. The H–H bond distances in the H_2 adsorptions on $C_{169}Pt(ce)$ and $C_{169}Pt(c)$ and on $C_{169}Pt(w)$ are 0.75 and 2.29 Å, respectively. The PtC bond distances between Pt and the carbon atoms of C_2H_4 in the C_2H_4 adsorption are about 2.3 Å. The PtH bond distances in the H_2 adsorptions on $C_{169}Pt(ce)$ and $C_{169}Pt(c)$ and on $C_{169}Pt(w)$ are about 2.7 and 1.7 Å, respectively. The PtC bond distances between Pt and its nearest carbon atoms of the SWCNT are about 2.0 Å. The numbers in parentheses are the PtC bond distances of the isolated $C_{169}Pt$ without adsorption, the C=C bond distance in the isolated free C_2H_4, and the H–H bond distance of the isolated free H_2.

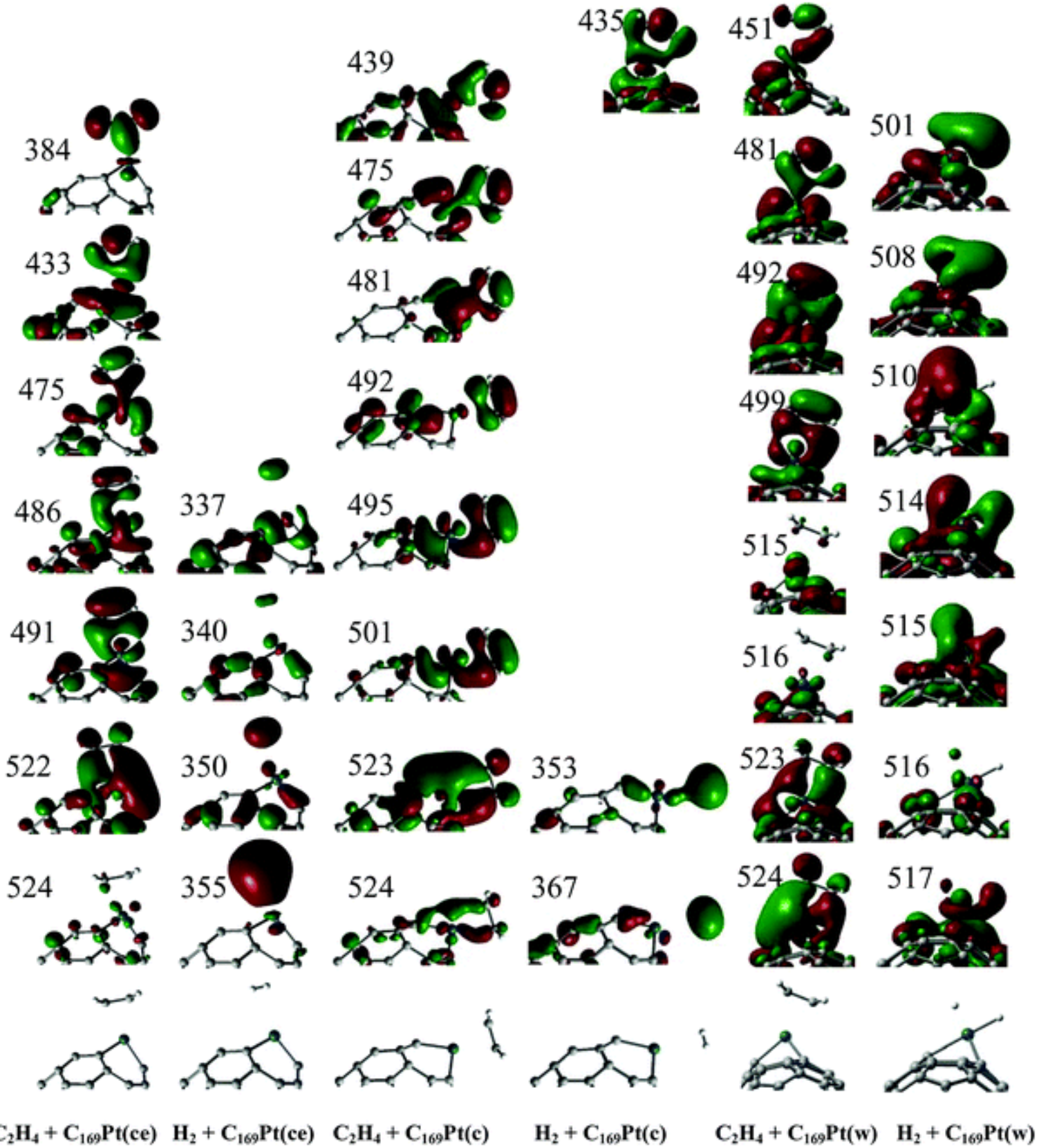

Fig. 12 Portions of the molecular orbitals relevant to the interaction of the adsorbates, C_2H_4 and H_2, with the three kinds of the Pt-doped nanorods, $C_{169}Pt(ce)$, $C_{169}Pt(c)$, and $C_{169}Pt(w)$. The numbers beside the molecular orbitals are the orbital indexes. The critical geometries of these structures are shown in Fig. 11.

The adsorption of C_2H_4 on the Pt atom in the three Pt-doped nanorods is physisorption with C–Pt

distances *ca*. 2.30 Å. As the adsorption site changes from the end-caps of $C_{169}Pt$(ce) and $C_{169}Pt$(c) to the middle of the sidewall of $C_{169}Pt$(w), the CC bond distance in C_2H_4 gets longer, and Pt–C bond distances between C_2H_4 and Pt get shorter, perhaps indicating the strength of the interaction between C_2H_4 and the Pt-doped SWCNTs in this ascending order: $C_{169}Pt(ce) < C_{169}Pt(c) < C_{169}Pt(w)$. However, this conclusion based on structure analysis alone does not agree with the data in Table 1: the adsorption energy of C_2H_4 is the smallest on $C_{169}Pt$(w) and the largest on $C_{169}Pt$(c). The trend of the adsorption strengths of C_2H_4 on the Pt-doped SWCNTs is the compromise of the weakening of the C=C double bond in C_2H_4, the electrostatic attraction between the two carbon atoms of C_2H_4 and Pt, and the repulsion between the C_2H_4 and the SWCNT. It is also interesting to note that the geometries of the adsorptions of C_2H_4 on the Pt atom at the end-cap of the Pt-doped SWCNTs are very similar to those on the Pt-doped fullerene, $C_{59}Pt$,[21e] which should possess similar adsorption strengths.

Overall, the adsorptions of H_2 and C_2H_4 get stronger as the adsorption site changes from the hemispheric cap to the sidewall of the SWCNT, as manifested by the relevant MOs in Fig. 12 and the adsorption energies in Table 1.

IV. Conclusions

Within DFT, the electronic structures and chemical reactivity of the SWCNT rods C_{170} and C_{180}, the Pt-doped SWCNT rods $C_{169}Pt$(ce), $C_{169}Pt$(c), and $C_{169}Pt$(w) have been studied in detail. According to the analyses, we have reached the following conclusions:

1. There indeed exist localized electronic states on the caps of the SWCNT rods as confirmed by the DOS, the LDOS, and the frontier MOs. The circular *cis*-polyene chain between the cap and the sidewall of the SWCNT is chemically active.
2. The ground state of the Pt-doped SWCNT rod is a singlet.
3. The doping of Pt in the SWCNT rod results in localized electronic states at Pt, thus rendering Pt as the active center in chemical reactions, particularly for the wall-doped $C_{169}Pt$(w). The Pt-doped SWCNT rod with Pt at the end of the cap, $C_{169}Pt$(ce), can be used as a chemical sensor, since the doping of Pt enhances the sensitivity of the cap in interaction with the substrate due to the Pt 5d orbitals and the charge transfer from Pt to the carbon atoms. In Pt-doped SWCNT rods, Pt is essentially acting as Pt^+, because of the electron transfer of about one electron from Pt to the carbon atoms.
4. The doping of Pt in the middle of the sidewall of the nanorod has stronger interaction with the adsorbates (*e.g.*, H_2 and C_2H_4) than the nanorods with the doping of Pt at the hemispheric caps. This further suggests that the Pt-doped SWCNT has stronger adsorbing capacity than the Pt-doped fullerene. However, this phenomenon has to be investigated for systems involving other metals.

In summary, present DFT studies reveal that doping produces localized active centers, thus enhancing the chemical reactivity of the SWCNTs (with hemispherically capped ends). Our studies point to new directions for future applications of the SWCNTs in catalysis, chemic sensor, surface science, and nanotube chemistry.

Acknowledgements

The financial support from the Natural Sciences and Engineering Research Council (NSERC) of Canada

is gratefully acknowledged. WestGrid and C-HORSE have provided the necessary computational resources. L.V.L. gratefully acknowledges the Gladys Estella Laird and the Charles A. McDowell fellowships from the Department of Chemistry at the University of British Columbia.

References

1 (*a*) S. Iijima and T. Ichihashi, *Nature*, 1993, **363**, 603 [Links]; (*b*) D. S. Bethune, C.-H. Kiang, M. S. de Vries, G. Gorman, R. Savoy, J. Vazquez and R. Beyers, *Nature*, 1993, **363**, 605 [Links].

2 (*a*) S. Niyogi, M. A. Hamon, H. Hu, B. Zhao, P. Bhowmik, R. Sen, M. E. Itkis and R. C. Haddon, *Acc. Chem. Res.*, 2002, **35**, 1105 [Links]; (*b*) T. Hermraj-Benny, S. Banerjee and S. S. Wong, *Chem. Mater.*, 2004, **16**, 1855 [Links]; (*c*) J.-M. Nhut, P. Nguyen, C. Pham-Huu, N. Keller and M.-J. Ledoux, *Catal. Today*, 2004, **91**, 91 [Links]; (*d*) J. Zhang, H. Zou, Q. Qing, Y. Yang, Q. Li, Z. Liu, X. Guo and Z. Du, *J. Phys. Chem. B*, 2003, **107**, 3712 [Links].

3 (*a*) T. Yamabe, M. Imade, M. Tanaka and T. Sato, *Synth. Met.*, 2001, **117**, 61 [Links]; (*b*) X. Lu, F. Tian, Y. Feng, X. Xu, N. Wang and Q. Zhang, *Nano Lett.*, 2002, **2**, 1325 [Links]; (*c*) J. Li, Y. Zhang and M. Zhang, *Chem. Phys. Lett.*, 2002, **364**, 328 [Links]; (*d*) J. Cioslowski, N. Rao and D. Moncrieff, *J. Am. Chem. Soc.*, 2002, **124**, 8485 [Links]; (*e*) T. Kar, B. Akdim, X. Duan and R. Pachter, *Chem. Phys. Lett.*, 2004, **392**, 176 [Links]; (*f*) M. Zhao, Y. Xia, J. P. Lewis and L. Mei, *J. Phys. Chem. B*, 2004, **108**, 9599 [Links]; (*g*) S. Gustavsson, A. Rosén, H. Grennberg and K. Bolton, *Chem.-Eur. J.*, 2004, **10**, 2223 [Links]; (*h*) E. Joselevich, *ChemPhysChem*, 2004, **5**, 619 [Links]; (*i*) Z. Zhou, M. Steigerwald, M. Hybertsen, L. Brus and R. Friesner, *J. Am. Chem. Soc.*, 2004, **126**, 3597 [Links]; (*j*) T. Yumura, K. Hirahara, S. Bandow, K. Yoshizawa and S. Iijima, *Chem. Phys. Lett.*, 2004, **386**, 38 [Links].

4 (*a*) D. L. Carroll, P. Redlich, P. M. Ajayan, J. C. Charlier, X. Blase, A. De Vita and R. Car, *Phys. Rev. Lett.*, 1997, **78**, 2811 [Links]; (*b*) Z. Klusek, P. Kowalczyk and P. Byszewski, *Vacuum*, 2001, **63**, 145 [Links]; (*c*) M. Shiraishi and M. Ata, *Synth. Met.*, 2002, **128**, 235 [Links]; (*d*) K. A. Dean and B. R. Chalamala, *J. Vac. Sci. Technol., B*, 2003, **21**, 868 [Links]; (*e*) H. Kim, J. Lee, S.-J. Kahng, Y.-W. Son, S. B. Lee, C.-K. Lee, J. Ihm and Y. Kuk, *Phys. Rev. Lett.*, 2003, **90**, 216107 [Links].

5 (*a*) X. Blase, L. X. Bbenedict, E. L. Shirley and S. G. Louie, *Phys. Rev. Lett.*, 1994, **72**, 1878 [Links]; (*b*) Y. H. Lee, S. G. Kim and D. Tománek, *Phys. Rev. Lett.*, 1997, **78**, 2393 [Links]; (*c*) T. Yaguchi and T. Ando, *J. Phys. Soc. Jpn.*, 2001, **70**, 1327 [Links]; (*d*) T. Yaguchi and T. Ando, *J. Phys. Soc. Jpn.*, 2002, **71**, 2224 [Links]; (*e*) J. Jiang, J. Dong and D. Y. Xing, *Phys. Rev. B*, 2002, **65**, 245418 [Links]; (*f*) S. Compernolle, L. Chibotaru and A. Ceulemans, *J. Chem. Phys.*, 2003, **119**, 2854 [Links]; (*g*) L. Chico and W. Jasklski, *Phys. Rev. B*, 2004, **69**, 085406 [Links]; (*h*) G. Y. Guo, K. C. Chu, D.-S. Wang and C.-G. Duan, *Phys. Rev. B*, 2004, **69**, 205416 [Links].

6 P. M. Ajayan and O. Z. Zhou, in *Carbon Nanotubes Synthesis, Structure, Properties, and Applications*, ed. M. S. Dresselhaus, G. Dresselhaus and Ph. Avoutis, Springer, Berlin, 2001.

7 (*a*) P. Avouris, *Acc. Chem. Res.*, 2002, **35**, 1026 [Links]; (*b*) R. D. Antonov and A. T. Johnson, *Phys. Rev. Lett.*, 1999, **83**, 3274 [Links]; (*c*) M. S. Fuhrer, J. Nygård, L. Shih, M. Forero, Y.-G. Yoon, M. S. C. Mazzoni, H. J. Choi, J. Ihm, S. G. Louie, A. Zettl and P. L. McEuen, *Science*, 2000, **288**, 494 [Links].

8 (*a*) J. Kong, N. R. Franklin, C. Zhou, M. G. Chapline, S. Peng, K. Cho and H. Dai, *Science*, 2000, **287**, 622 [Links]; (*b*) P. G. Collins, K. Bradley, M. Ishigami and A. Zettl, *Science*, 2000, **287**, 1801 [Links]; (*c*) A. Goldoni, R. Larciprete, L. Petaccia and S. Lizzit, *J. Am. Chem. Soc.*, 2003, **125**, 11329 [Links].

9 O. Zhou, H. Shimoda, B. Gao, S. Oh, L. Fleming and G. Yue, *Acc. Chem. Res.*, 2002, **35**, 1045 [Links].

10 W. B. Choi, D. S. Chung, J. H. Kang, H. Y. Kim, Y. W. Jin, I. T. Han, Y. H. Lee, J. E. Jung, N. S. Lee, G. S. Park and J. M. Kim, *Appl. Phys. Lett.*, 1999, **75**, 3129 [Links].

11 P. Serp, M. Corrias and P. Kalck, *Appl. Catal., A*, 2003, **253**, 337 [Links].

12 (*a*) S. Botti, R. Ciardi, L. De Dominicis, L. S. Asilyan, R. Fantoni and T. Marolo, *Chem. Phys. Lett.*, 2003, **378**, 117 [Links]; (*b*) S. Tatsuura, M. Furuki, Y. Sato, I. Iwasa, M. Tian and H. Mitsu, *Adv. Mater.*, 2003, **15**, 534 [Links]; (*c*) S. Y. Set, H. Yaguchi, Y. Tanaka and M. Jablonski, *J. Lightwave Technol.*, 2004, **22**, 51 [Links]; (*d*) A. G. Rozhin, Y. Sakakibara, M. Tokumoto, H. Kataura and Y. Achiba, *Thin Solid Films*, 2004, **464–465**, 368 [Links].

13 (*a*) N. Hamada, S.-I. Sawada and A. Oshiyama, *Phys. Rev. Lett.*, 1992, **68**, 1579 [Links]; (*b*) M. S. Dresselhaus, G. Dresselhaus and P. C. Eklund, *Science of Fullerenes and Carbon Nanotubes*, Academic Press Inc., San Diego, ch. 19, 1995.

14 I. W. Chiang, B. E. Brinson, A. Y. Huang, P. A. Willis, M. J. Bronikowski, J. L. Margrave, R. E. Smalley and R. H. Hauge, *J. Phys. Chem. B*, 2001, **105**, 8297 [Links].

15 (*a*) E. T. Mickelson, C. B. Huffman, A. G. Rinzler, R. E. Smalley, R. H. Hauge and J. L. Margrave, *Chem. Phys. Lett.*, 1998, **296**, 188 [Links]; (*b*) P. J. Boul, J. Liu, E. T. Mickelson, C. B. Huffman, L. M. Ericson, I. W. Chiang, K. A. Smith, D. T. Colbert, R. H. Hauge, J. L. Margrave and R. E. Smalley, *Chem. Phys. Lett.*, 1999, **310**, 367 [Links]; (*c*) M. Holzinger, O. Vostrowsky, F. H. Hirsch, M. Kappes, R. Weiss and F. Jellen, *Angew. Chem., Int. Ed.*, 2001, **40**, 4002 [Links]; (*d*) J. L. Bahr and J. L. Tour, *Chem. Mater.*, 2001, **13**, 3823 [Links]; (*e*) J. L. Bahr, J. Yang, D. V. Kosynkin, M. J. Bronikowski, R. E. Smalley and J. M. Tour, *J. Am. Chem. Soc.*, 2001, **123**, 6536 [Links]; (*f*) V. Georgakilas, K. Kordatos, M. Prato, D. M. Guldi, M. Holzinger and A. Hirsch, *J. Am. Chem. Soc.*, 2002, **124**, 760 [Links]; (*g*) P. Umek, J. W. Seo, K. Hernadi, A. Mrzel, P. Pechy, D. D. Mihailovic and L. Forr, *Chem. Mater.*, 2003, **15**, 4751 [Links]; (*h*) J. L. Stevens, A. Y. Huang, H. Peng, I. W. Chiang, V. N. Khabashesku and J. L. Margrave, *Nano Lett.*, 2003, **3**, 331 [Links]; (*i*) H. Peng, L. B. Alemany, J. L. Margrave and V. N. Khabashesku, *J. Am. Chem. Soc.*, 2003, **125**, 15174 [Links]; (*j*) H. Hu, B. Zhao, M. A. Hamon, K. Kamaras, M. E. Itkis and R. C. Haddon, *J. Am. Chem. Soc.*, 2003, **125**, 14893 [Links]; (*k*) S. Banerjee, M. G. C. Kahn and S. S. Wong, *Chem.-Eur. J.*, 2003, **9**, 1898 [Links]; (*l*) B. Zhao, H. Hu and R. C. Haddon, *Adv. Funct. Mater.*, 2004, **14**, 71 [Links]; (*m*) L. Zhang, V. U. Kiny, H. Pesng, J. Zhu, R. F. M. Lobo, J. L. Margrave and V. N. Khabashesku, *Chem. Mater.*, 2004, **16**, 2055 [Links].

16 (*a*) M. A. Hamon, J. Chen, H. Hu, Y. Chen, M. E. Itkis, A. M. Rao, P. C. Eklund and R. C. Haddon, *Adv. Mater.*, 1999, **11**, 834 [Links]; (*b*) J. Zhang, H. Zou, Q. Qing, Y. Yang, Q. Li, Z. Liu, X. Guo and Z. Du, *J. Phys. Chem. B*, 2003, **107**, 3712 [Links].

17 J. L. Bahr and J. M. Tour, *J. Mater. Chem.*, 2002, **12**, 1952 [Links].

18 (*a*) P. M. Ajayan, V. Ravikumar and J.-C. Charlier, *Phys. Rev. Lett.*, 1998, **81**, 1437 [Links]; (*b*) M. Igami, T. Nakanishi and T. Ando, *J. Phys. Soc. Jpn.*, 1999, **68**, 716 [Links]; (*c*) M. Igami, T. Nakanishi and T. Ando, *Physica B (Amsterdam)*, 2000, **284**, 1746 [Links]; (*d*) A. V. Krasheninnikov and K. Nordlund, *Phys. Solid State*, 2002, **44**, 470 [Links]; (*e*) J.-C. Charlier, *Acc. Chem. Res.*, 2002, **35**, 1063 [Links]; (*f*) A. V. Krasheninnikov and K. Nordlund, *J. Vac. Sci. Technol., B*, 2002, **20**, 728 [Links]; (*g*) A. J. Lu and B. C. Pan, *Phys. Rev. Lett.*, 2004, **92**, 105504 [Links]; (*h*) V. V. Belavin, L. G. Bulusheva and A. V. Okotrub, *Int. J. Quantum Chem.*, 2004, **96**, 239 [Links]; (*i*) L. Valentini, F. Mercuri, I. Armentano, C. Cantalini, S. Picozzi, L. Lozzi, S. Santucci, A. Sgamellotti and J. M. Kenny, *Chem. Phys. Lett.*, 2004, **387**, 356 [Links]; (*j*) L. V. Liu, W. Q. Tian and Y. A. Wang, *J. Phys. Chem. B*, 2006, **110**, 1999 [Links].

19 (*a*) D. L. Carroll, Ph. Redlich, X. Blase, J.-C. Charlier, S. Curran, P. M. Ajayan, S. Roth and M. Rühle, *Phys. Rev. Lett.*, 1998, **81**, 2332 [Links]; (*b*) W. Han, Y. Bando, K. Kurashima and T. Sato, *Chem. Phys. Lett.*, 1999, **299**, 368 [Links]; (*c*) S. Peng and K. Cho, *Nano Lett.*, 2003, **3**, 513 [Links]; (*d*) M. Zhao, Y. Xia, J. Lewis and R. Zhang, *J. Appl. Phys.*, 2003, **94**, 2398 [Links]; (*e*) A. V. Nikulkina and P. N. D'yachkov, *Russ. J. Inorg. Chem.*, 2004, **49**, 430.

20 (*a*) Ph. Lambin, A. A. Lucas and J. C. Charlier, *J. Phys. Chem. Solids*, 1997, **58**, 1833 [Links]; (*b*) H. J. Choi, J. Ihm, S. G. Louie and M. L. Cohen, *Phys. Rev. Lett.*, 2000, **84**, 2917 [Links]; (*c*) M. B. Nardelli, J.-L. Fattebert, D. Orlikowski, C. Roland, Q. Zhao and J. Bernholc, *Carbon*, 2000, **38**, 1703 [Links]; (*d*) H.-F. Hu, Y.-B. Li and H.-B. He, *Diamond Relat. Mater.*, 2001, **10**, 1818 [Links]; (*e*) L. G. Zhou and S. Q. Shi, *Carbon*, 2003, **41**, 579 [Links]; (*f*) Y. Miyamoto, A. Rubio, S. Berber, M. Yoon and D. Tománek, *Phys. Rev. B*, 2004, **69**, 121413 [Links].

21 (*a*) D. E. Clemmer, J. M. Hunter, K. B. Shelimov and M. F. Jarrold, *Nature*, 1994, **372**, 248 [Links]; (*b*) W. Branz, I. M. L. Billas, N. Malinowski, F. Tast, M. Heinebrodt and T. P. Martin, *J. Chem. Phys.*, 1998, **109**, 3425 [Links]; (*c*) J. M. Poblet, J. Muñoz, K. Winkler, M. Cancilla, A. Hayashi, C. B. Lebrilla and A. L. Balch, *Chem. Commun.*, 1999, 493 [Links]; (*d*) Q. Kong, Y. Shen, L. Zhao, J. Zhuang, S. Qian, Y. Li, Y. Lin and R. Cai, *J. Chem. Phys.*, 2002, **116**, 128 [Links]; (*e*) A. Hayashi, Y. Xie, J. M. Poblet, J. M. Campanera, C. B. Lebrilla and A. L. Balch, *J. Phys. Chem. A*, 2004, **108**, 2192 [Links].

22 (*a*) C. Ding, J. Yang, X. Cui and C. T. Chan, *J. Chem. Phys.*, 1999, **111**, 8481 [Links]; (*b*) I. M. L. Billas, C. Massobrio, M. Boero, M. Parrinello, W. Branz, F. Tast, N. Malinowski, M. Heinebrodt and T. P. Martin, *Comput. Mater. Sci.*, 2000, **17**, 191 [Links].

23 A. De Vita, J.-Ch. Charlier, X. Blase and R. Car, *Appl. Phys. A*, 1999, **68**, 283 [Links].

24 R. Tamura and M. Tsukada, *Phys. Rev. B*, 1995, **52**, 6015 [Links].

25 (*a*) P. Hohenberg and W. Kohn, *Phys. Rev.*, 1964, **136**, B864 [Links]; (*b*) W. Kohn and L. J. Sham, *Phys. Rev.*, 1965, **40**, A1133 [Links]; (*c*) R. G. Parr and W. Yang, *Density-functional theory of atoms and molecules*, Oxford University Press, New York, 1989.

26 A. D. Becke, *Phys. Rev. A*, 1988, **38**, 3098 [Links].

27 (*a*) J. P. Perdew, J. A. Chevary, S. H. Vosko, K. A. Jackson, M. R. Pederson, D. J. Singh and C. Fiolhais, *Phys. Rev. B*, 1992, **46**, 6671 [Links]; (*b*) J. P. Perdew, K. Burke and Y. Wang, *Phys. Rev. B*, 1996, **54**, 16533 [Links].

28 (*a*) R. Ditchfield, W. J. Hehre and J. A. Pople, *J. Chem. Phys.*, 1971, **54**, 724 [Links]; (*b*) W. J. Hehre, R. Ditchfield and J. A. Pople, *J. Chem. Phys.*, 1972, **56**, 2257 [Links]; (*c*) P. C. Hariharan and J. A. Pople, *Mol. Phys.*, 1974, **27**, 209 [Links]; (*d*) M. S. Gordon, *Chem. Phys. Lett.*, 1980, **76**, 163 [Links].

29 P. J. Hay and W. R. Wadt, *J. Chem. Phys.*, 1985, **82**, 299 [Links].

30 (*a*) Y. Sheng, D. G. Musaev, K. S. Reddy, F. E. McDonald and K. Morokuma, *J. Am. Chem. Soc.*, 2002, **124**, 4149 [Links]; (*b*) W. Q. Tian and Y. A. Wang, *J. Org. Chem.*, 2004, **69**, 4299 [Links].

31 (*a*) A. D. Becke, *J. Chem. Phys.*, 1993, **98**, 5648 [Links]; (*b*) C. Lee, W. Yang and R. G. Parr, *Phys. Rev. B*, 1988, **37**, 785 [Links]; (*c*) B. Miehlich, A. Savin, H. Stoll and H. Preuss, *Chem. Phys. Lett.*, 1989, **157**, 200 [Links].

32 (*a*) A. E. Reed and F. Weinhold, *J. Chem. Phys.*, 1983, **78**, 4066 [Links]; (*b*) J. E. Carpenter, PhD thesis, University of Wisconsin, Madison, WI, 1987; (*c*) J. E. Carpenter and F. Weinhold, *J. Mol. Struct. (THEOCHEM)*, 1988, **169**, 41 [Links]; (*d*) A. E. Reed, L. A. Curtiss and F. Weinhold, *Chem. Rev.*, 1988, **88**, 899 [Links].

33 M. J. Frisch*et al.*, *GAUSSIAN 03 (Revision B.05)*, Gaussian, Inc., Wallingford, CT, 2004.

34 T. Yumura, S. Bandow, K. Yoshizawa and S. Iijima, *J. Phys. Chem. B*, 2004, **108**, 11426 [Links].

35 G. Mpourmpakis, G. E. Froudakis, A. N. Andriotis and M. Menon, *Appl. Phys. Lett.*, 2005, **87**, 193105 [Links].

Footnotes

† The HTML version of this article has been enhanced with colour images.

‡ Permanent address: State Key Laboratory of Theoretical and Computational Chemistry, Institute of Theoretical Chemistry, Jilin University, Changchun, Jilin 130023, China.